



Impacts of the IOD-associated temperature and salinity anomalies on the intermittent equatorial undercurrent anomalies

Junde Li^{1,2} · Chujin Liang² · Youmin Tang^{2,3} · Xiaohui Liu² · Tao Lian² · Zheqi Shen² · Xiaojing Li²

Received: 26 January 2017 / Accepted: 8 October 2017 / Published online: 11 November 2017
© The Author(s) 2017. This article is an open access publication

Abstract The study of Equatorial Undercurrent (EUC) has attracted a broad attention in recent years due to its strong response and feedback to the Indian Ocean Dipole. In this paper, we first produce a high-quality simulation of three-dimensional temperature, salinity and zonal current simulation from 1982 to 2014, using a high-resolution ocean general circulation model. On this basis, with two sensitivity experiments, we investigate the role of temperature and salinity anomalies in driving and enhancing the EUC during the positive IOD events by examining the variation of the EUC seasonal cycle and diagnosing the zonal momentum budget along the equatorial Indian Ocean. Our results show that during January–March, the EUC can appear along the entire equatorial Indian Ocean in all years, but during August–November, the EUC can appear and reach the eastern Indian Ocean only during the positive IOD events. The zonal momentum budget analysis indicates that the pressure gradient force contributes most to the variation of the eastward acceleration of zonal currents in the subsurface. During the positive IOD events, strong negative subsurface temperature anomalies exist in the eastern Indian Ocean, with negative surface salinity anomalies in the central and eastern Indian Ocean, resulting in a large pressure gradient force to drive EUC during the August–November. Further,

the results of two sensitivity experiments indicate that the temperature anomalies significantly impact the pressure gradient force, playing a leading role in driving the EUC, while the surface salinity anomalies can secondarily help to intensify the eastward EUC through increasing the zonal density gradient in the eastern Indian Ocean and impacting the vertical momentum advection in the subsurface.

Keywords Equatorial Undercurrent · Indian Ocean Dipole · ROMS · Zonal momentum budget

1 Introduction

The Indian Ocean Dipole (IOD) is a major ocean–atmosphere coupled mode of inter-annual climate variability in the tropical Indian Ocean (Saji et al. 1999; Webster et al. 1999), characterized by opposite sea surface temperature (SST) anomalies in the eastern (90°E – 110°E , 10°S – 0°S) and western (50°E – 70°E , 10°S – 10°N) tropical Indian Ocean. An IOD event usually develops from June, and peaks at September–November (SON) (Saji et al. 1999). During a positive IOD (pIOD) event, easterly wind anomalies occur over the central equatorial Indian Ocean with negative rainfall and SST anomalies off the Sumatra-Java coast, and vice versa for a negative IOD (nIOD) event (Saji and Yamagata 2003a). Due to the strong equatorial wind anomalies and SST anomalies across the Indian Ocean basin, IOD can significantly modulate the atmospheric circulation, which results in a series of climate anomalies including droughts, floods and also effects on societies and economics such as agriculture, water resources, forestry wildfires, and the spread of insects and waterborne diseases over the Indian Ocean and the surrounding areas (Ashok et al. 2001; Saji and Yamagata 2003b; Behera et al. 2005; Cai et al. 2009,

✉ Youmin Tang
ytang@unbc.ca

¹ College of Oceanic and Atmospheric Sciences, Ocean University of China, Qingdao, China

² State Key Lab of Satellite Ocean Environment Dynamics, Second Institute of Oceanography, State Oceanic Administration, Hangzhou, China

³ Environmental Science and Engineering, University of Northern British Columbia, Prince George, BC, Canada

2011; Ummenhofer et al. 2009; Hashizume et al. 2012; Feng et al. 2014; Guo et al. 2015; Yao et al. 2016).

In the equatorial Indian Ocean, strong westerly winds dominate in boreal spring and fall during the monsoon transition seasons, and drive the eastward surface currents known as Wyrtki Jets (Wyrtki 1973; Reppin et al. 1999). These jets trap the momentum from which the zonal winds input into the oceans in the upper 100 m and significantly influence the climate via horizontal heat, salt and mass transport in the tropical Indian Ocean (Murtugudde et al. 2000). The Equatorial Undercurrent (EUC) flows eastward in the thermocline under the surface current that flows westward or weakly eastward (Schott and McCreary Jr. 2001; Chen et al. 2015, 2016). The EUC in the Indian Ocean is significantly different from that in the other oceans. In the equatorial Pacific and Atlantic Oceans, the prevailing easterly trade winds exist all year that drive a quasi-permanent eastward EUC, however, the EUC is transient in the Indian Ocean (McPhaden 1986). On seasonal time scales, the EUC is most prominent during boreal winter and spring, particularly from February to April, and with a secondary and much weaker peak in boreal late summer to early fall (Knox 1976; McPhaden 1982; Reppin et al. 1999; Izumo 2005; Iskandar et al. 2009). On interannual time scales, the summer-fall EUC in the central and eastern equatorial Indian Ocean becomes stronger during the pIOD events than during normal period (Reppin et al. 1999; Swapna and Krishnan 2008; Iskandar et al. 2009), which feeds and intensifies the upwelling off the Sumatra-Java coast, producing a positive feedback to the decrease of SST in this region (Thompson et al. 2006; Nyadapro and McPhaden 2014; Zhang et al. 2014; Chen et al. 2016).

Over the last decades, there have been a number of works to study the relationships between the transient EUC and IOD events, using observations, models and reanalysis products. The spatial structure, the transport, the seasonal to interannual variability of EUC and its potential role in the IOD development have been investigated (Grodsky et al. 2001; Zhang et al. 2014; Chen et al. 2015). Several dynamical hypotheses that drive the anomalous EUC during the pIOD events have also been proposed (Masson et al. 2004; Swapna and Krishnan 2008; Iskandar et al. 2009; Krishnan and Swapna 2009; Chen et al. 2015). It was found that both directly wind-driven Kelvin and Rossby waves and eastern boundary-reflected Rossby waves significantly contribute to the formation of EUC during the pIOD events (Iskandar et al. 2009; Chen et al. 2015). The intensified summer monsoon winds during pIOD events are also found to be able to amplify the easterlies in the equatorial eastern and central Indian Ocean, and generate an eastward zonal pressure gradient force responsible for the anomalous EUC in the thermocline (Han et al. 2004; Swapna and Krishnan 2008; Krishnan and Swapna 2009).

While significant progresses have been made in understanding the EUC and in investigating the impact of IOD on it, one fundamental issue is still not clear, namely that, what factor or physical process plays dominant role in sustaining the intermittent Equatorial Undercurrent? One typical question is, as we will find in later discussion, why the EUC can only pass across around 70°E and propagate to the eastern Indian Ocean during the positive IOD events and vanish at the equatorial central Indian Ocean during other years? It was argued that the salinity anomalies may have a very important impact on the EUC during the 1997 IOD event (Masson et al. 2004). This is probably because the anomalous zonal currents driven by the easterlies advect the fresh water from the Bay of Bengal and the Sumatra-Java coast into the central equatorial Indian Ocean to change the sea-water density distribution (Thompson et al. 2006; Grunseich et al. 2011; Zhang et al. 2013; Li et al. 2016). For example, Masson et al. (2003, 2004) designed sensitivity experiments to investigate the impacts of salinity on the pressure gradient and vertical mixing and concluded the importance of the IOD-deduced salinity anomalies to the EUC.

While there were considerable works to examine the transient EUC features and possible mechanisms during the IOD events through exploring either temperature or salinity anomalies or wave dynamics, there were few efforts in literature to put them in an integral framework to examine these anomalies and their interactions and connections, i.e., integrating temperature, salinity, density, and currents as a whole system to examine the EUC and the IOD. A further examination of the impact of temperature and salinity anomalies on the EUC in such a way is also a necessary step towards a fully understanding to the EUC dynamics involving transient surface zonal winds, zonal pressure gradient, monsoon, equatorial Kelvin and Rossby waves. In particular, such a study can allow us to shed light on the dominant factor of EUC anomalies.

In this paper, we will use a high-resolution eddy-resolving ocean general circulation model (OGCM), together with observation and reanalysis data including the Research Moored Array for African–Asian–Australian monsoon analysis and prediction (RAMA) (McPhaden et al. 2009), European Centre for Medium-Range Weather Forecasts (ECMWF) Ocean Reanalysis System 4 (ORAS4) and Argo floats, to investigate the EUC seasonal and interannual variability, as well as the impact of IOD on these features. Emphasis is placed on the examination of contributions of different physical process to EUC by dynamical diagnosis of the zonal momentum budget along the equator during the IOD events. To our knowledge, it is the first attempt to quantify the contribution of temperature and salinity to the zonal momentum budget of the EUC during the pIOD events. The goal of our study is to try to offer a comprehensive understanding to the spatial structure and seasonal evolution of the

EUC, and the dynamical processes of the summer–autumn EUC extending eastward, during the pIOD events.

The rest of the paper is structured as follows: Sect. 2 describes data, model and methods. In Sect. 3, we present the validation of the model results using observations and reanalysis dataset. Section 4 discusses the seasonal characteristics of the EUC. In Sect. 5, we investigate the dynamics of the EUC based on the zonal momentum budget. Finally, in Sect. 6, we provide a summary and discussion.

2 Data and methods

2.1 OGCM description and experiments

The OGCM used in the study is based on the Regional Ocean Modeling System (ROMS) developed by Rutgers University. It solves the primitive equations on a free-surface and terrain-following coordinates system (Shchepetkin and McWilliams 2005), which has been widely used in the study of oceanic processes and simulations (Liu et al. 2014; Li et al. 2016). The model domain is within the tropical Indian Ocean (30°E – 110°E , 30°S – 30°N) with a horizontal resolution of $1/8^{\circ}$ and 32 vertical levels. We use the vertical S-coordinate surface ($\theta_s = 3.0$) and bottom control parameters ($\theta_b = 0.3$), and the newly defined vertical transformation equation ($V\text{transform}=2$) and stretching function ($V\text{stretching}=4$) of the vertical levels. The surface boundary layer with higher vertical resolution is defined as the critical depth using a stretching control parameter $h_c = 100$ m. We use the ETOPO2, which is a 2 arc-minute global relief model of Earth's surface that integrates land topography and the ocean bathymetry dataset, to provide the topography (Smith and Sandwell 1997). It is smoothed with the slope parameter $r = \frac{\nabla h}{h} = 0.2$ and the maximum depth is 5000 m. We use the mixed open boundary conditions along the eastern and southern boundaries, whereas the northern and western boundaries are closed.

The model was initiated from the oceanic state in December of 1978 from simple ocean data assimilation (SODA) reanalysis release 2.2.4 (Carton and Giese 2008). Then, the ocean model is forced by 6-hourly surface atmospheric variables over January 1979–March 2011 from the Climate Forecast System Reanalysis (CFSR) 93.0 (Saha et al. 2010) and over April 2011–December 2014 from Climate Forecast System Version 2 (CFSv2) (Saha et al. 2014). The lateral boundaries are constrained with a 30-day time-scale relaxation to monthly averaged temperature, salinity, velocities and sea surface height (SSH) from SODA over January 1979–December 2010 and from Estimating the Circulation and Climate of the Ocean (ECCO) reanalysis product over January 2011–December 2014. We add monthly climatological continental runoffs from the climate and global

dynamics laboratory (CGDL) (Dai and Trenberth 2002) and apply no relaxation to the observed SSS climatology in the experiment, which can produce more realistic seasonal and interannual SSS variations (Li et al. 2016). The model creates a restart file that restores all the model states at the end of each year and is used as an initial condition for next year. The outputs are stored at 1 day interval. Considering the spin-up issue, we discard the first 3 years and only analyse the outputs from January 1982 to December 2014 in this study. With the above settings and configurations, the model has a good simulation for the tropical Indian Ocean SSTA and SSSA, particularly a good simulation of Dipole Mode Index (DMI), as validated in Li et al. (2016). In following discussion, this model is also found to have a good capability in characterizing EUC features, thus it is a useful tool to study the structure and dynamics of the EUC.

In order to evaluate the impact of temperature and salinity anomalies on the EUC, we set up two sensitivity experiments. The first experiment is designed to remove the impact of temperature anomalies along the equatorial Indian Ocean (5°S – 5°N) during the five pIOD years (1982, 1994, 1997, 2006, 2012) but to keep salinity anomalies unchanged, which is called temperature nudging experiment. This is implemented by nudging the monthly climatological temperature at a 30-day time-scale in the whole water column, which is the averaged temperature of the control run over 33 years, and meanwhile nudging the monthly salinity of the control run during the pIOD events. All other setting and configurations, as well as the atmospheric forcing are the same as the above control run. The second experiment, called salinity nudging experiment, is similar to the first one but for salinity, i.e., removing the anomalous salinity impact by nudging the monthly climatological salinity, and meanwhile nudging the monthly temperature of the control run.

2.2 Zonal momentum budget

To examine the EUC evaluation and its physical process, we start from the governing equations of the zonal momentum budget, as written below:

$$\underbrace{\frac{\partial u}{\partial t}}_{Du/dt} = - \underbrace{\left(u \frac{\partial u}{\partial x} + v \frac{\partial u}{\partial y} + w \frac{\partial u}{\partial z} \right)}_{\text{Adv}} + fv - \underbrace{\frac{1}{\rho} \frac{\partial p}{\partial x}}_{\text{PGF}} + \underbrace{\frac{\partial}{\partial z} \left(A_v \frac{\partial u}{\partial z} \right)}_{\text{Diff}} + D_u \quad (1)$$

where u , v and w are zonal, meridional and vertical velocities, respectively; f is the Coriolis parameter, p is the pressure, A_v is the vertical diffusion coefficient, D_u is the horizontal diffusive terms. The Coriolis force is zero at the equator thus its effect is neglected in the following discussion. Equation (1) indicates that the tendency of zonal momentum (Du/dt) is balanced by the zonal, meridional

and vertical advection (Adv), zonal pressure gradient force (PGF) and the horizontal and vertical diffusion (Diff) (Nagura and McPhaden 2014).

The budget analysis of Eq. (1) is important to understand dynamic and physical process of the current, allowing to examine the major contributions to the current anomalies. There are usually two strategies to diagnosis the budget. One is the off-line approach using observation or model outputs, and the other is the on-line one directly integrating the model and examining each item of Eq. (1). In this study, we use the latter approach, which can avoid the truncation errors from the spatial and temporal differential and other uncertain factors, and strictly keep the budget balance among all items. The daily average of each item of Eq. (1) is stored for following analysis.

2.3 Datasets

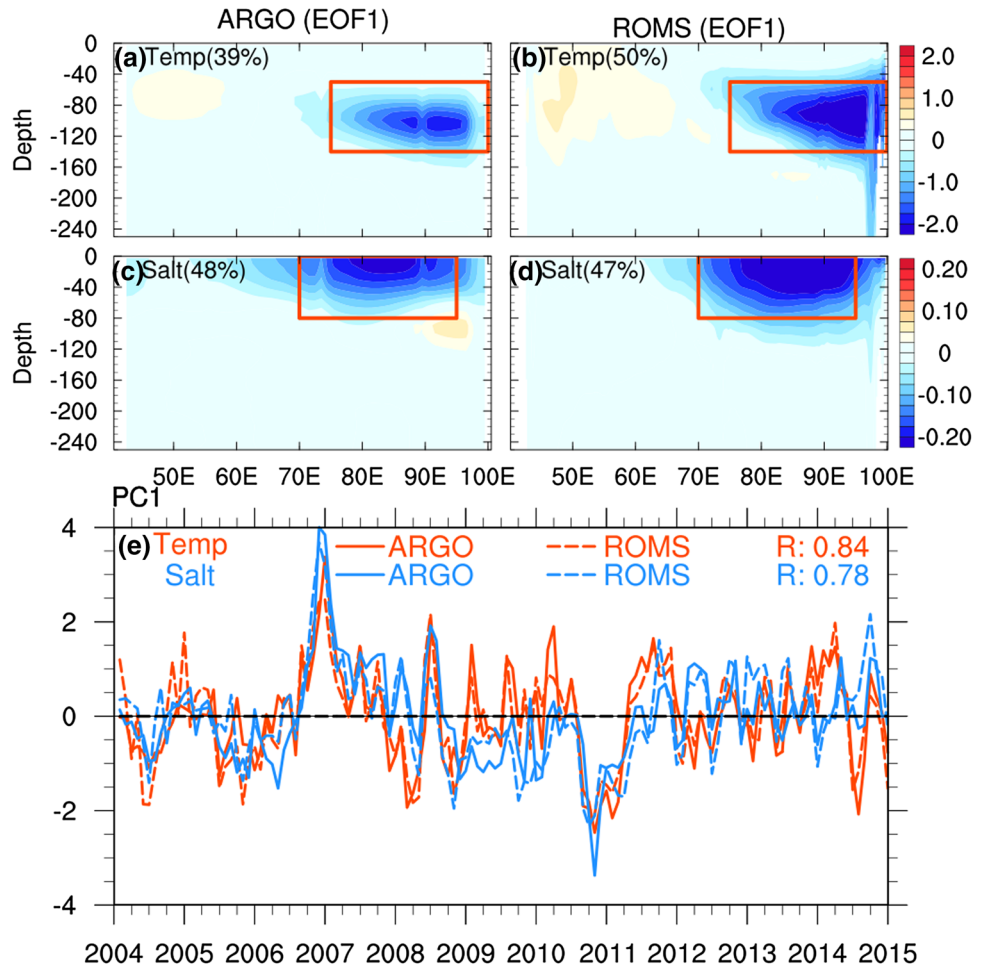
We use the monthly gridded ARGO data from January 2004 to December 2014 to validate the temperature and salinity simulation in the model. These data are provided by the Scripps Institution of Oceanography with a resolution of

$1^\circ \times 1^\circ$ (Roemmich and Gilson 2009). Monthly currents from the ORAS4 ocean reanalysis from January 1982 to December 2014 are used to validate the temporal variability and spatial structure of the currents in the model. ORAS4 has a horizontal resolution of $1^\circ \times 1^\circ$ and 42 vertical levels of which the first 14 levels are within the upper 150 m (Balmaseda et al. 2013). We also use the in situ current observations from the acoustic Doppler current profiler (ADCP) of two moorings to examine the zonal velocity of the model simulations. These moorings are deployed in the research moored array for African–Asian–Australian monsoon analysis and prediction (RAMA) (McPhaden et al. 2009). The vertical resolution of the mooring at 0° , 80.5°E and 0° , 90°E are 5 and 10 m, respectively. Monthly averaged zonal velocity data from November 2004 to October 2008 for 80.5°E and November 2000 to March 2009 for 90°E are used in this study.

3 Interannual variability of EUC

An EOF analysis is conducted on both the ARGO and ROMS temperature and salinity profile in the upper 250 m along

Fig. 1 Spatial patterns of the first EOF mode and their corresponding principal components (PCs) for the monthly temperature and salinity anomalies from 2004 to 2014 along the equatorial Indian Ocean (0.5°S – 0.5°N , 40°E – 100°E). **a, b** First EOF modes for temperature obtained from ARGO and ROMS, respectively. **c, d** Same as **a, b**, but for salinity. The red boxes in **a–d** show the central locations of anomalies (**a, b** 75°E – 100°E , 50 – 140 m; **c, d** 70°E – 95°E , 0 – 80 m). **e** Corresponding PCs of the first EOF mode for temperature (red line) and salinity (blue line) from ARGO (solid line) and ROMS (dashed line). R are the correlation coefficients of PCs between ARGO and ROMS



the equatorial Indian Ocean (0.5°S – 0.5°N , 40°E – 100°E). Figure 1a, b show the first EOF mode (EOF1) of temperature from ARGO and ROMS, accounting for 39 and 50% of the total variance, respectively. As can be seen, both EOF1 modes have a very similar pattern characterized by negative anomalies within the 50–140 m layer between 75°E – 100°E . The time series of their EOF1, i.e., the first principal component (PC1), are shown in Fig. 1e, presenting a good relationship with their correlation coefficient of 0.84. In the same way, we examine the salinity simulation and find negative anomalies occurred over upper 80 m between 70°E – 95°E in EOF1 mode of ARGO and ROMS salinity, as shown in Fig. 1c, d, which accounts for 48 and 47% of the total variance, respectively. The correlation coefficient between their PC1 is 0.78 as shown in Fig. 1e. Figure 1e also shows a strong interannual oscillation in both temperature and salinity, which positively peaks at 2006 corresponding with a pIOD year and vice versa for the nIOD year of 2010. This is because the cooling in the eastern Indian Ocean is associated with a decrease in salinity during a positive IOD event and vice versa in a negative IOD phase. During the pIOD events, the anomalous easterlies drive anomalous zonal currents that advect fresh water from the Sumatra-Java coast and the Bay of Bengal into the central equatorial Indian Ocean, which decrease the salinity (Thompson et al. 2006; Zhang et al. 2013; Li et al. 2016).

Fig. 2 Spatial pattern of the first EOF mode and its corresponding principal component time series for the monthly zonal current anomalies from 1982 to 2014 along the equatorial Indian Ocean (0.5°S – 0.5°N , 40°E – 100°E). **a, b** The first EOF patterns from ORAS4 and ROMS, respectively. The red boxes in **a, b** show the central locations of anomalies (60°E – 95°E , 0–80 m). **c** Time series of the first EOF principal component (PC1) from ORAS4 (red line) and ROMS (blue line). The correlation coefficient of PC1 between ORAS4 and ROMS is indicated

To examine the simulation of ROMS zonal velocity, we conduct an EOF analysis for ORAS4 and ROMS after removing their seasonal cycle. Positive anomalies exist at the equatorial upper 80 m between 60°E – 95°E in both ORAS4 and ROMS EOF1, as shown in Fig. 2a, b. These strong eastward zonal currents are dominated by the Wyrtki Jets appearing during the monsoon transition seasons. Figure 2c presents the PC1 of the zonal velocity from the model and the reanalysis, respectively, showing a good relationship between them with a statistically significant correlation coefficient at 99% confidence level. This suggests that the simulated current can be a reliable product for use and analysis.

Shown in Fig. 3 is the equatorial zonal velocity of the upper 200 m at 80.5°E and 90°E , respectively, from RAMA, the model and ORAS4. As can be seen in this figure, the model displays a pattern very similar to that of RAMA and ORAS4. For example, Fig. 3b shows strong eastward zonal currents dominating the upper 80 m during the boreal spring and autumn of each year at 80.5°E , particularly in 2005, which are very consistent with the observations in Fig. 3a, c.

Figure 3 also shows that the EUC has a transient seasonal variation in the depth between 80 and 160 m. For example, the observation and reanalysis data show that when weakly eastward subsurface zonal currents at 80.5°E are dominant during the boreal winter-spring, these currents can also appear at the boreal autumn at this location at some

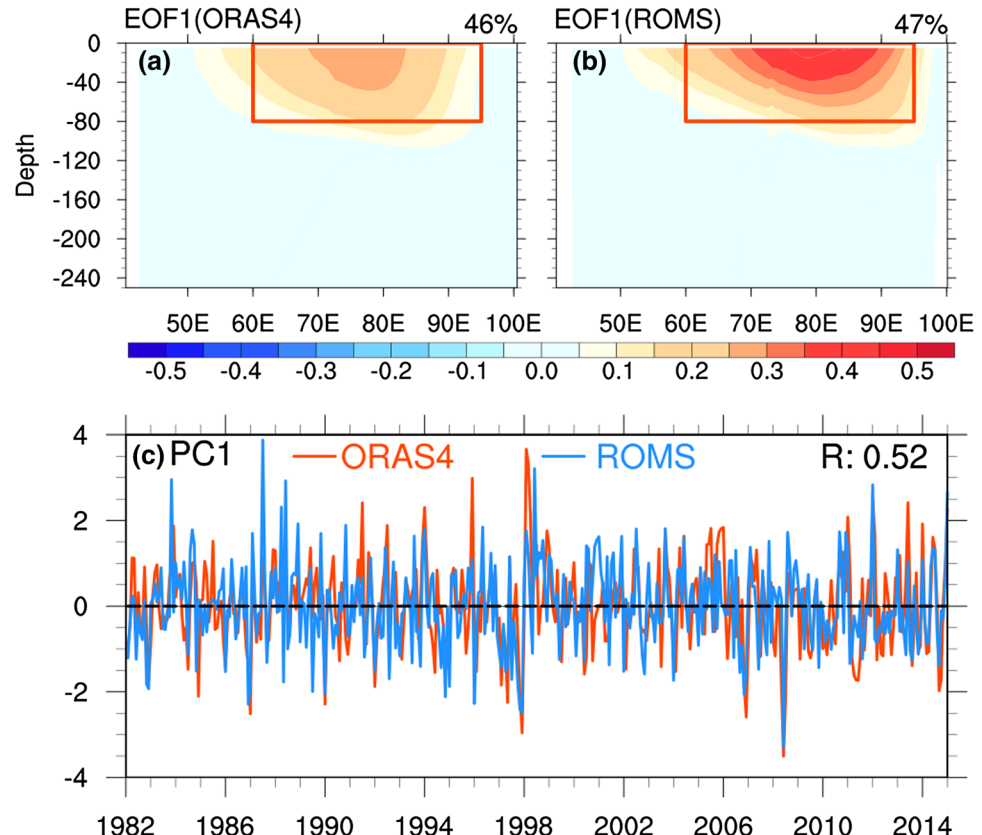
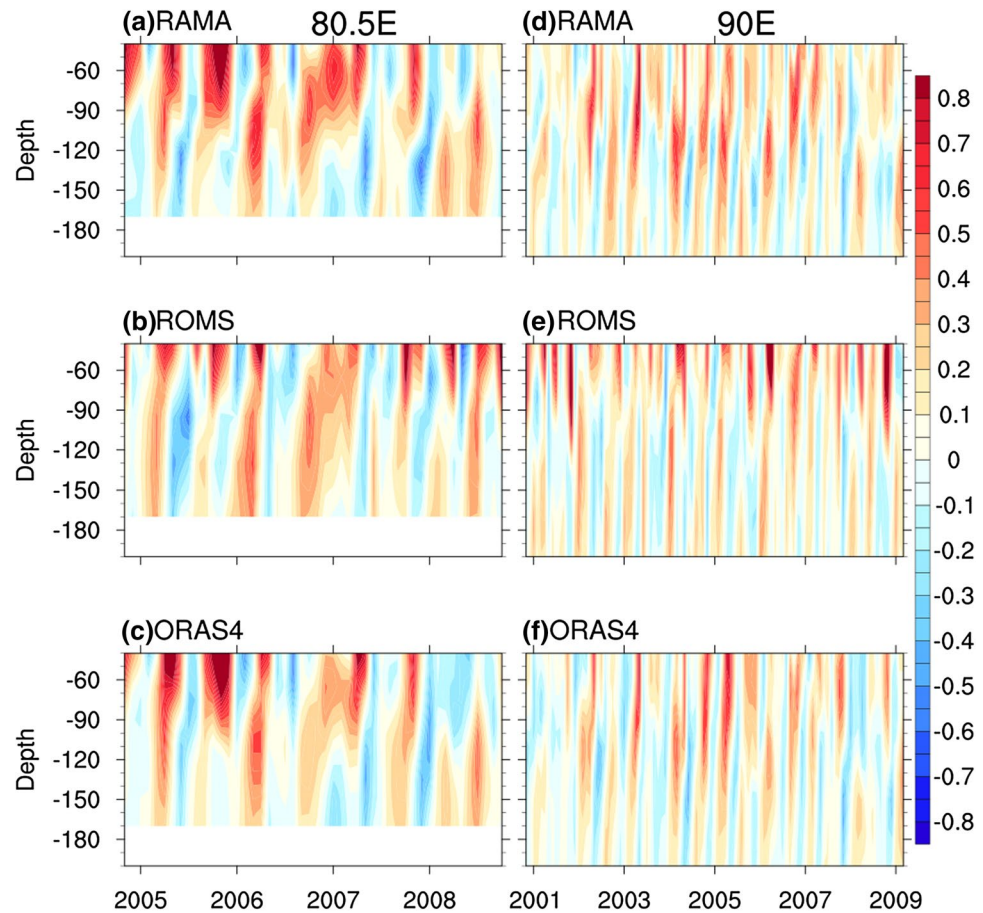


Fig. 3 Monthly averaged zonal currents at 80.5°E , 0.5°S – 0.5°N (**a**–**c**) and 90°E , 0.5°S – 0.5°N (**d**–**f**). The top panel (**a**, **d**), middle panel (**b**, **e**), and bottom panel (**c**, **f**) are for RAMA, ROMS and ORAS4, respectively



circumstances such as the pIOD year of 2006. This transient feature is well reproduced in the model. This is the same for 90°E . Thus, this model can not only reproduce the strong Wyrtki Jets in the surface (0–80 m) but also present the transient EUC in the subsurface (80–160 m).

A further validation of the current simulation is performed by EOF analysis. Shown in Fig. 4a–d are the EOF first two modes and corresponding time series of the zonal currents along the equator at 80.5°E and 90°E , respectively, for the ORAS4 and the model for the period from 1982 to 2014. The first two modes explain over 85% of total variance for model and observation for both latitudes.

Comparison between ORAS4 and the model (ROMS) in Fig. 4a–d reveals that their leading EOF modes at the two latitudes are very similar to each other. In agreement with previous study (Nyadjro and McPhaden 2014), EOF1 shows a dominant pattern like Wyrtki Jets that occur in the upper 80 m (Fig. 4a, c) whereas the EOF2 shows a EUC-like structure, with weaker eastward subsurface currents appearing at about 80 m, peaking at 100 m, and disappearing at 160 m (Fig. 4b, d). The eastward subsurface zonal currents between 80 and 160 m, are defined as EUC in this study. It should be noted that the depth of EUC is not exactly defined in a range of 60–170 m or

16–26 °C equivalently, with some differences for different researchers (Swapna and Krishnan 2008; Iskandar et al. 2009; Krishnan and Swapna 2009; Nyadjro and McPhaden 2014; Zhang et al. 2014; Chen et al. 2015; McPhaden et al. 2015). Our definition can separate the EUC from the surface Wyrtki Jets and also capture the EUC maximum at the subsurface. The PC1 and PC2 are shown in Fig. 4e–h. As can be seen, significant seasonal cycle is featured in the model and ORAS4 for both latitudes.

Compared with the PC1 and EOF1, the model has a better simulation in the EOF2 and PC2, although the correlation of PC1 between the model and ORAS4 is also statistically significant at the confidence level of 95%. Comparison also reveals that the surface currents are stronger in ROMS than in ORAS4. To investigate the possible reason for the stronger current in ROMS, we compared the surface zonal winds used in ROMS and in ORAS4, and found them comparable. However, the mixed layer depths in ROMS are a bit deeper. Another reason is that both the LMD (Large, McWilliams and Doney scheme) frictional parameterizations and vertical mixing coefficient used in ROMS are probably different from ORAS4, resulting in that the vertical mixing in ROMS is weaker than that in ORAS4. This would impede the surface momentum

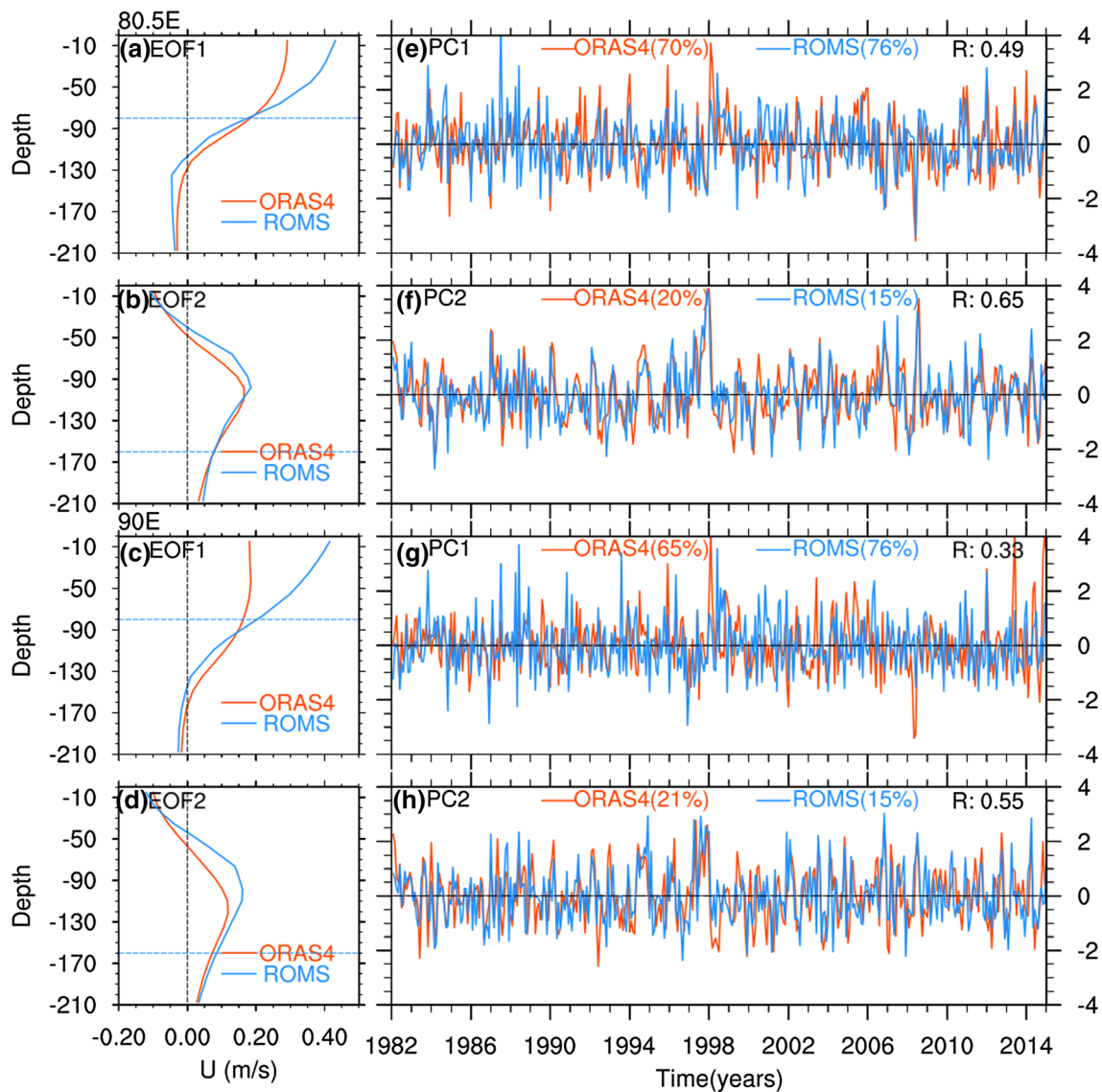


Fig. 4 Spatial function of EOF1 and EOF2 of ORAS4 and ROMS zonal currents at 80.5°E, 0.5°S–0.5°N (**a**, **b**) and 90°E, 0.5°S–0.5°N (**c**, **d**). The corresponding PC1 and PC2 of ORAS4 and ROMS zonal currents at 80.5°E, 0.5°S–0.5°N (**e**, **f**) and 90°E, 0.5°S–0.5°N (**g**, **h**).

Solid red lines and blue lines in each panel represent ORAS4 and ROMS, respectively. Dash blue lines in (**a**, **c**) and (**b**, **d**) represent the depth of 80 and 160 m respectively. The correlation coefficients of PC1 and PC2 between ORAS4 and ROMS are indicated in (**e**–**h**)

penetrating downward and induce stronger currents in the surface layer.

4 Seasonal cycle of EUC

To examine the seasonal variations of EUC, we average monthly zonal currents between 80 m and 160 m along the equatorial Indian Ocean (5°S–5°E). Shown in Fig. 5 are the time-longitude diagrams of the above averaged EUC from the climatological mean of 33 years from 1982 to 2014, the average of positive IOD years (1982, 1994, 1997, 2006,

2012) and the average of negative IOD years (1984, 1996, 1998, 2005, 2010), respectively. Usually, during the boreal winter-spring season, the northeastern seasonal winds dominate the northern Indian Ocean, and the averaged winds along the equatorial Indian Ocean are westward (Schott and McCreary Jr. 2001). In this season, the EUC is confined within 2°S–2°N. It appears across the whole equatorial Indian Ocean in January, strengthens in February and peaks in March and then disappears in April, in all years. During the boreal summer (May–Jun–Jul), the subsurface zonal currents reverse the direction and EUC almost disappears in the whole equatorial Indian Ocean. During the boreal fall,

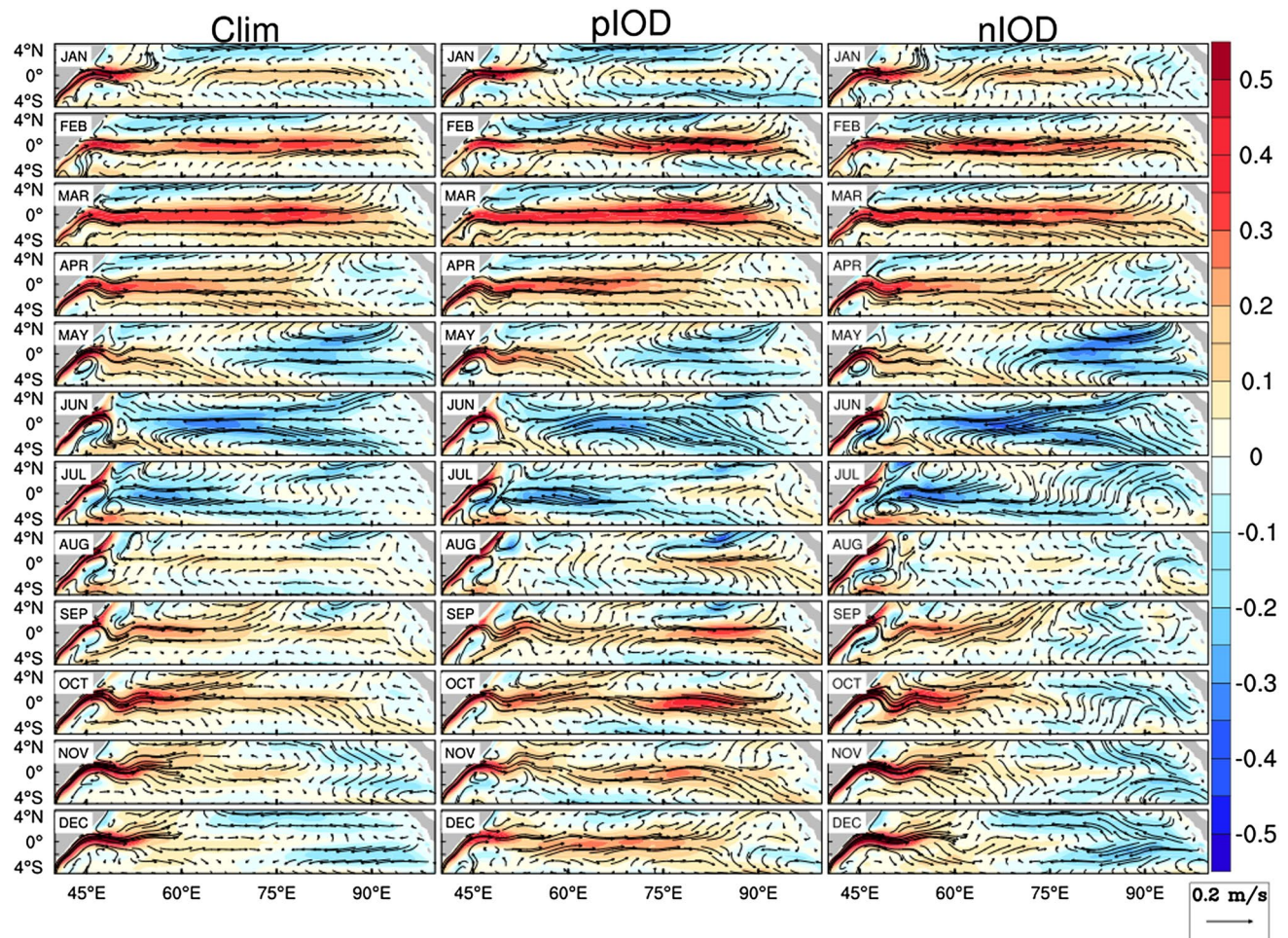


Fig. 5 Seasonal variation of EUC using ROMS monthly averaged currents for climatology (left) during 1982–2014, composed positive IOD events (1982, 1994, 1997, 2006 and 2012) (middle) and

negative IOD events (1984, 1996, 1998, 2005 and 2010) (right). The color shows the magnitude of the zonal component in m/s

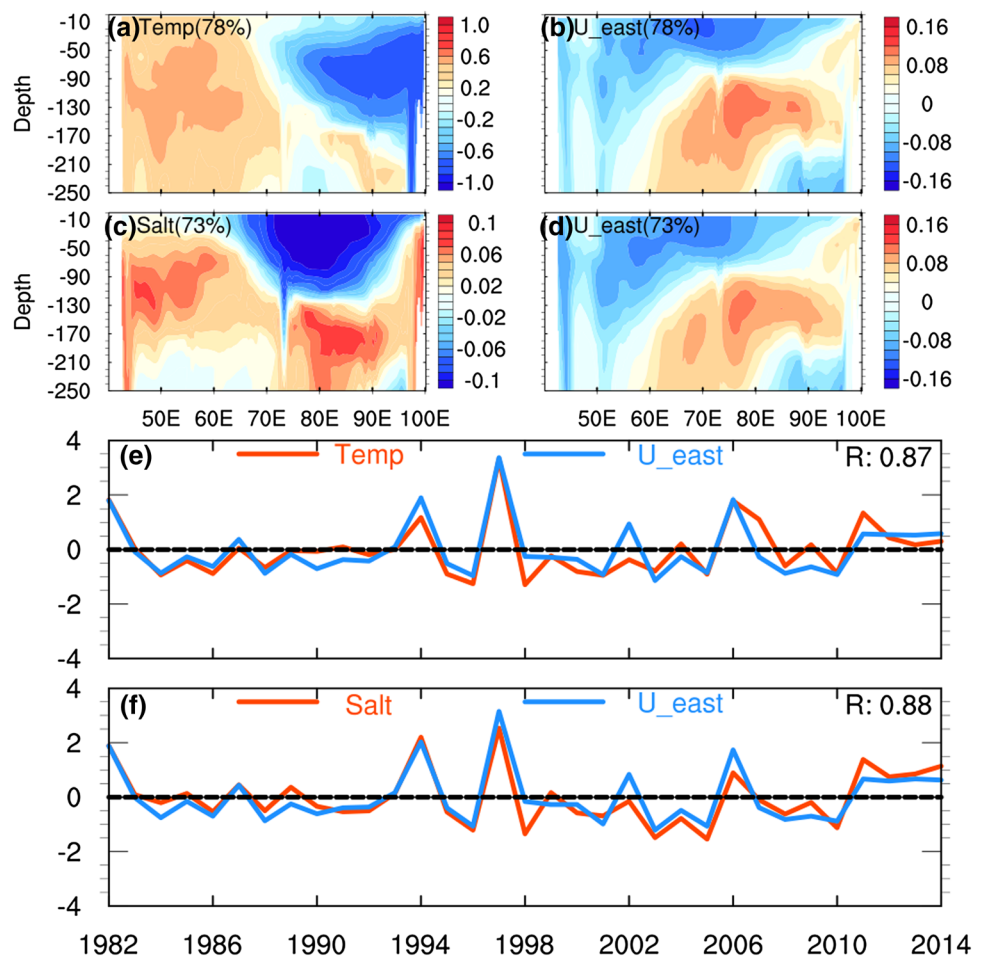
the EUC reappears in the eastern equatorial Indian Ocean in pIOD years. Compared to the winter-spring EUC, the autumn EUC is weaker, particularly in the western equatorial Indian Ocean.

A significant feature in Fig. 5 is that the autumn EUC can transport eastward to the eastern equatorial Indian Ocean only in the pIOD years. In climatology and nIODs years, the EUC is usually terminated at around 60°E–70°E and cannot further transport eastward. It is interesting to examine the possible reasons. Usually, the ocean current anomalies are always accompanied by temperature and salinity anomalies. Figure 6a, b shows the leading SVD (singular value decomposition) mode (SVD1) between SON temperature and zonal current anomalies, which explains 78% of the total variance. As can be found, the significant temperature anomalies appear in the subsurface (50–140 m) over the eastern equatorial Indian Ocean (75°E–100°E), accompanied correspondingly by a negative zonal current anomaly

center in the surface (0–80 m) and a positive anomaly area in the subsurface (80–160 m). Consistent with the spatial distribution of SVD1, the time series of this leading mode are significantly correlated with a high correlation of 0.87, as shown in Fig. 6e. In the same way, we examine the relationships between SON salinity and zonal current anomalies. This leading mode is shown in Fig. 6c-d accounting for 73% of the total variance, indicating that the salinity anomalies are negative in the surface (0–80 m) over the central equatorial Indian Ocean and the zonal current anomalies are very similar to those in Fig. 6b. The correlation coefficient of the time series between the zonal current and the salinity is 0.88 as shown in Fig. 6f. Fig. 6e, f also shows that temperature and salinity anomalies vary in phase with zonal current anomalies, which positively peak at pIOD years (e.g., 1994, 1997 and 2006).

The coherent structure of temperature, salinity and the EUC anomalies can also be reflected by the composite

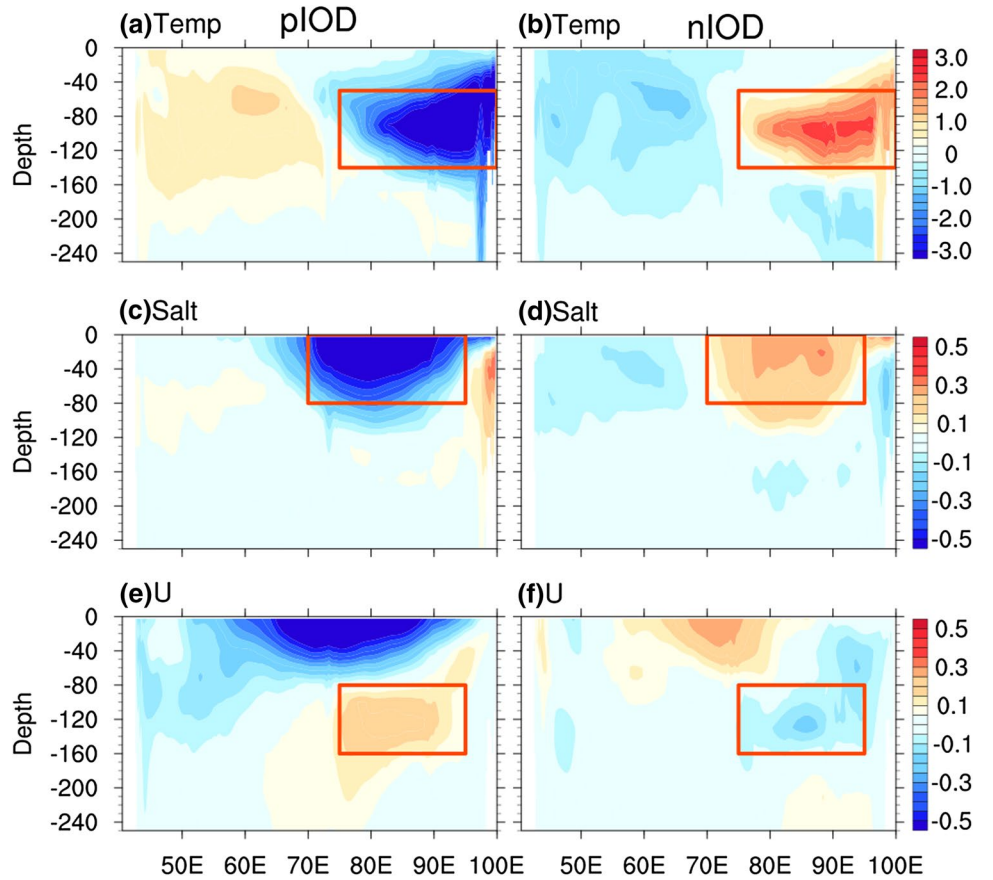
Fig. 6 Spatial patterns of the leading SVD mode and their corresponding time series between SON (Sep–Oct–Nov) temperature, salinity anomalies and SON zonal current anomalies from 1982 to 2014 along the equatorial Indian Ocean (0.5°S – 0.5°N , 40°E – 100°E). **a, b** Leading SVD mode of temperature and zonal current, respectively. **c, d** Same as **a, b**, but for salinity and zonal current. **e** Corresponding time series of the leading SVD mode for temperature (red line) and zonal current (blue line). R is the correlation coefficient. **f** Same as **e**, but for salinity and zonal current



analysis. Figure 7 shows the SON temperature, salinity and zonal current anomalies composite maps for the five positive and five negative IODs. The composited analysis is consistent with the EOF and SVD results as discussed above, namely that, the strong temperature anomalies appear in the subsurface of the eastern Indian Ocean whereas the negative current and salinity anomalies appear in the surface of the central equatorial Indian Ocean. During the pIOD events, strong upwelling in the eastern equatorial Indian Ocean leads to large negative temperature anomalies in the subsurface (Fig. 7a), and strong westward zonal currents driven by anomalous easterlies advect fresh water from the Sumatra–Java coast and the Bay of Bengal into the central and eastern equatorial Indian Ocean (Fig. 7c) (Thompson et al. 2006; Li et al. 2016). Note a weak eastward zonal current is visible under the strong westward anomalous surface current above 80 m during pIOD events, which is the autumn EUC with its core within 80–160 m between 75°E and 95°E , as shown in the red boxes in Fig. 7e. During the nIOD events, temperature, salinity, and zonal current anomalies also appear in the same location but in an opposite direction (Fig. 7b, d, f).

To examine the temporal evolution of EUC, we averaged the temperature, salinity and zonal current within the red boxes of Fig. 7. Figure 8 shows the monthly temperature, salinity and zonal current during a 3-year evolution of pIOD events, from 1 year before to 1 year after the IOD year for 5 positive and 5 negative composed IOD events, respectively. For comparison, a climatological seasonal cycle is also presented in Fig. 8. As we can see, there are no significant differences in temperature, salinity and zonal currents during boreal winter–spring between IOD years and climatology (Feb–Mar). For example, the peak value of EUC in this season has 0.26, 0.31 and 0.24 m/s for climatology, pIOD and nIOD years, respectively, as shown by the narrow grey bar in Fig. 8c. However, striking difference can be found in boreal autumn. During the pIOD events, the EUC peaks at about 0.27 m/s, and the differences of EUC reaches 0.15 m/s between the pIOD and climatology in the boreal autumn, as shown in the wide bar in Fig. 8c. In addition, both autumn temperature and salinity are lower by 2.3°C and 0.42 psu during pIOD events, respectively, compared with their climatology counterparts. Thus, we will focus on

Fig. 7 Composited SON mean temperature (**a**, **b**), salinity (**c**, **d**) and zonal current (**e**, **f**) anomalies averaged over 0.5°S–0.5°N for 5 positive IOD events (1982, 1994, 1997, 2006 and 2012) (left) and 5 negative IOD events (1984, 1996, 1998, 2005 and 2010) (right). The red boxes in (a-d) are the same as Fig. 1a-d, and red boxes in (e, f) indicate the central locations of EUC (75°E–95°E, 80–160 m)



the EUC anomalies at the boreal autumn in following diagnosis analysis.

5 Dynamics of EUC

5.1 Zonal momentum budget

As discussed in Sect. 2.2, we use the zonal momentum budget equation to examine the dynamics of EUC, and evaluate the contribution of each individual physical process to it. Applying Eq. (1) onto the equator and integrating it from the depth of 80–160 m, we can obtain the below equation after neglecting the Coriolis term at the equator,

$$\underbrace{\frac{d\bar{u}}{dt}}_{Du/dt} = \underbrace{-\left(\bar{u}\frac{\partial\bar{u}}{\partial x} + \bar{v}\frac{\partial\bar{u}}{\partial y} + \bar{w}\frac{\partial\bar{u}}{\partial z}\right)}_{Adv} - \underbrace{\frac{1}{\rho}\frac{\partial\bar{p}}{\partial x}}_{PGF} + \underbrace{\frac{\partial}{\partial z}\left(A_v\frac{\partial\bar{u}}{\partial z}\right) + \overline{D_u}}_{Diff} \quad (2)$$

where overbar in Eq. (2) denotes the depth integrated terms, namely $\bar{X} = \frac{1}{h_2-h_1} \int_{-h_2}^{-h_1} X dz$, with X denoting an variable.

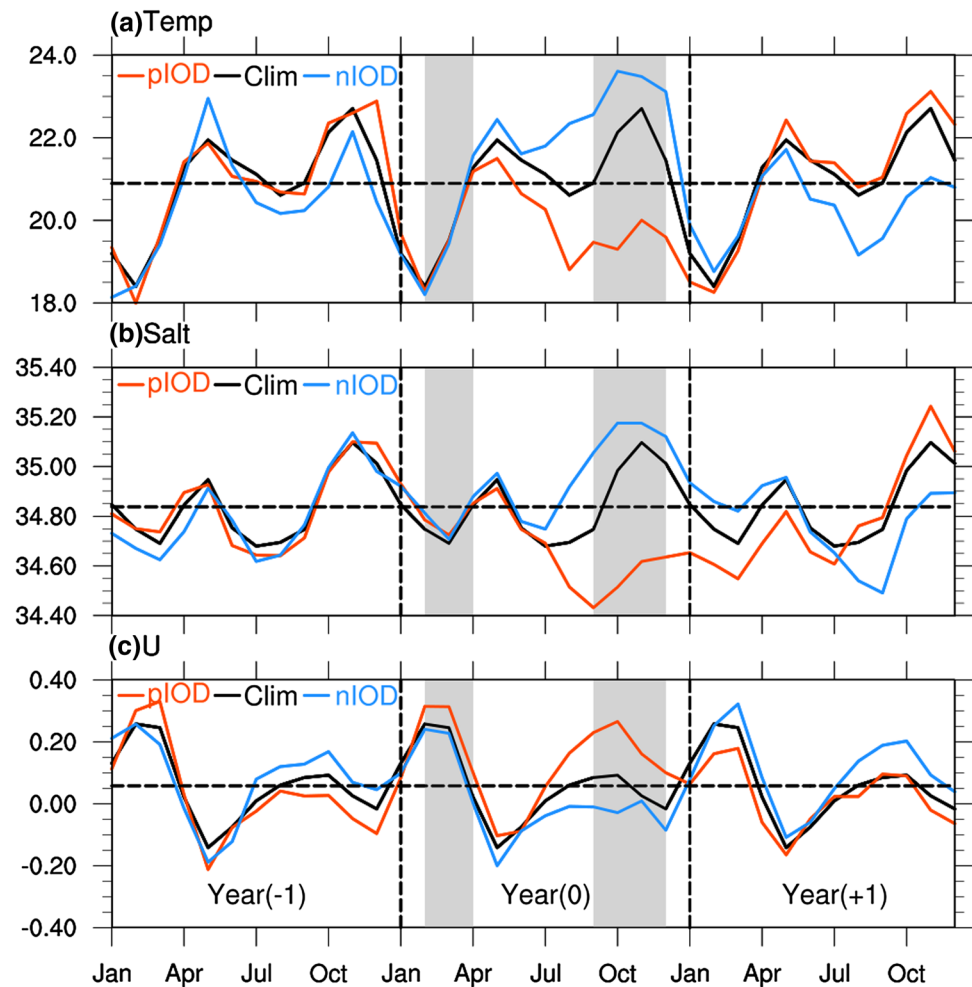
Here, we choose $h_1 = 80$ m and $h_2 = 160$ m, following the EUC definition discussed in Sect. 3. As described in the

previous studies (Nagura and McPhaden 2014), the diffusion term which represents the response of ocean to wind forcing is mainly trapped in the upper 100 m, and is thus negligible.

Figure 9 shows seasonal evolution of each term of Eq. (2) except for the diffusion term. As can be seen in Fig. 9a, b, the EUC ranges from 90°E to the western boundary in winter–spring but disappears in summer. Instead, the westward zonal currents occupy the whole equator from late April to middle July. In autumn, the EUC reappears but has a significant difference in its range and strength between normal years and pIOD events, as mentioned above. Namely, the EUC can only pass across 70°E to the eastern Indian Ocean in the pIOD years.

In the subsurface, the impact of wind stress is weak and the tendency of vertical integrated zonal current is mainly dominated by the pressure gradient force and horizontal and vertical advection. Figure 9c–h presents the seasonal variations of these dominant items, showing that the tendency of zonal current has similar seasonal characteristic as zonal current. In general, the pressure gradient force contributes most to its variation, and the advection term is relatively very small in most region of the equator except at the eastern boundary. In winter–spring, both the pressure gradient force and advection contribute to the increase of eastward

Fig. 8 Temporal evolution of temperature (a), salinity (b) and zonal current (c), averaged within the red boxes in Fig. 7, for climatology (black line), composited positive IOD events (1982, 1994, 1997, 2006 and 2012) (red line) and negative IOD events (1984, 1996, 1998, 2005 and 2010) (blue line) from the previous IOD year (-1), IOD year (0) to the following IOD year ($+1$). The horizontal dashed black line in a–c represents climatological mean temperature, salinity and zonal current, respectively. The wide grey bars in a–c indicate the months of September–November, and the narrow grey bars in a–c indicate February–March



zonal current, and the pressure gradient force plays a more important role in autumn than that in winter–spring. It is apparent that the pressure gradient force in autumn is much stronger in pIOD than in normal years, which is a main factor resulting in the intensification and eastward extension of the transient EUC in this season. Next, we will examine the variation of August–September for each term of Eq. (2) to further understand the process of transient EUC.

The composite of the zonal momentum budget components of August–September averaged over the 5 pIOD events is shown in Fig. 10a–d. For comparison, a similar climatological composite analysis is also conducted, as shown in Fig. 10e–h. As expected, the tendency of zonal current is negative in the upper layer of 80 m and positive in the subsurface (80–160 m) in the equatorial Indian Ocean during the pIOD events (Fig. 10a). However, the positive climatological tendency of zonal current only occurs in the upper 80 m, with a westward zonal current acceleration below (Fig. 10e). In pIOD years, positive pressure gradient force appears in the subsurface between 55°E and 85°E and becomes stronger in the surface east

of 85°E (Fig. 10b). In contrast, the climatological pressure gradient force is negative in the upper ocean and is very small in the subsurface (Fig. 10f). The total momentum advection has a relative small contribution to the eastward zonal current acceleration in the subsurface in pIOD years (Fig. 10c). Also, climatological advection leads to westward acceleration in the upper 20 m and eastward acceleration below (Fig. 10g). During the pIOD events, the vertical advection in the subsurface causes and accelerates eastward flow, which also contributes to intermittent autumn EUC (Fig. 10d). However, the positive vertical advection is constrained within the upper 80 m in the climatology (Fig. 10h).

In general, the tendency of climatological zonal current accelerates eastward in the upper 80 m and with an opposite sign in the subsurface, resulting the EUC weakened, even disappeared. Giving overall consideration to each component and comparing the results between pIOD and climatology, we can draw a conclusion that the autumn EUC is mainly driven by the eastward pressure gradient force in the

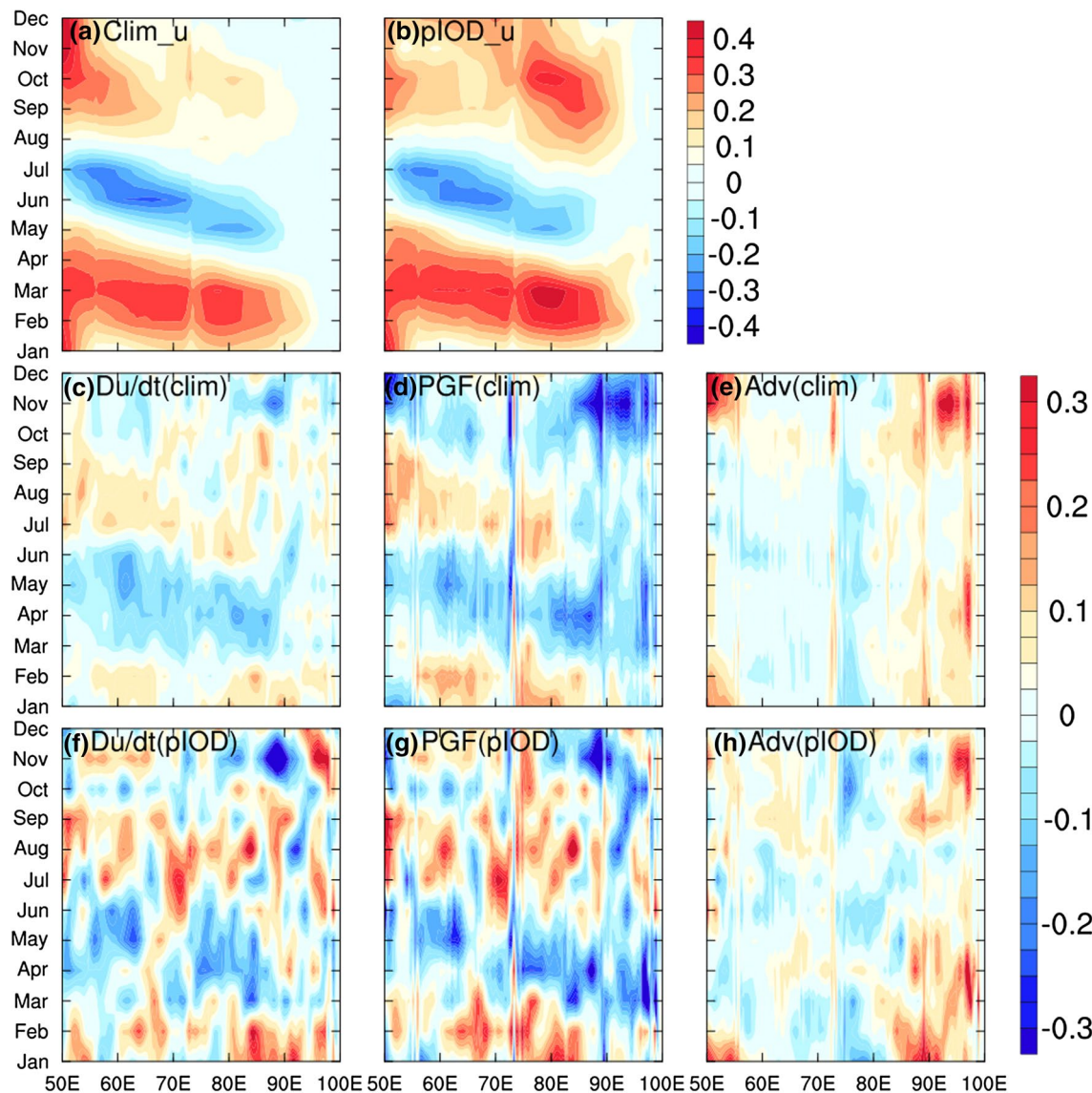


Fig. 9 Monthly evolution of the depth integrated (80–160 m) zonal current (upper) and zonal momentum budget components averaged over 0.5°S – 0.5°N for climatology (middle) and composited positive IOD events (1982, 1994, 1997, 2006 and 2012) (bottom). **a, c–e** Zonal current, the tendency of zonal current, the pressure gradient

force and advection for climatology, respectively. **b, f–h** Same as **a, c–e**, but for positive IOD events. The colors show the magnitude of the zonal current in m/s and zonal momentum budget components in 10^{-6} m/s^2

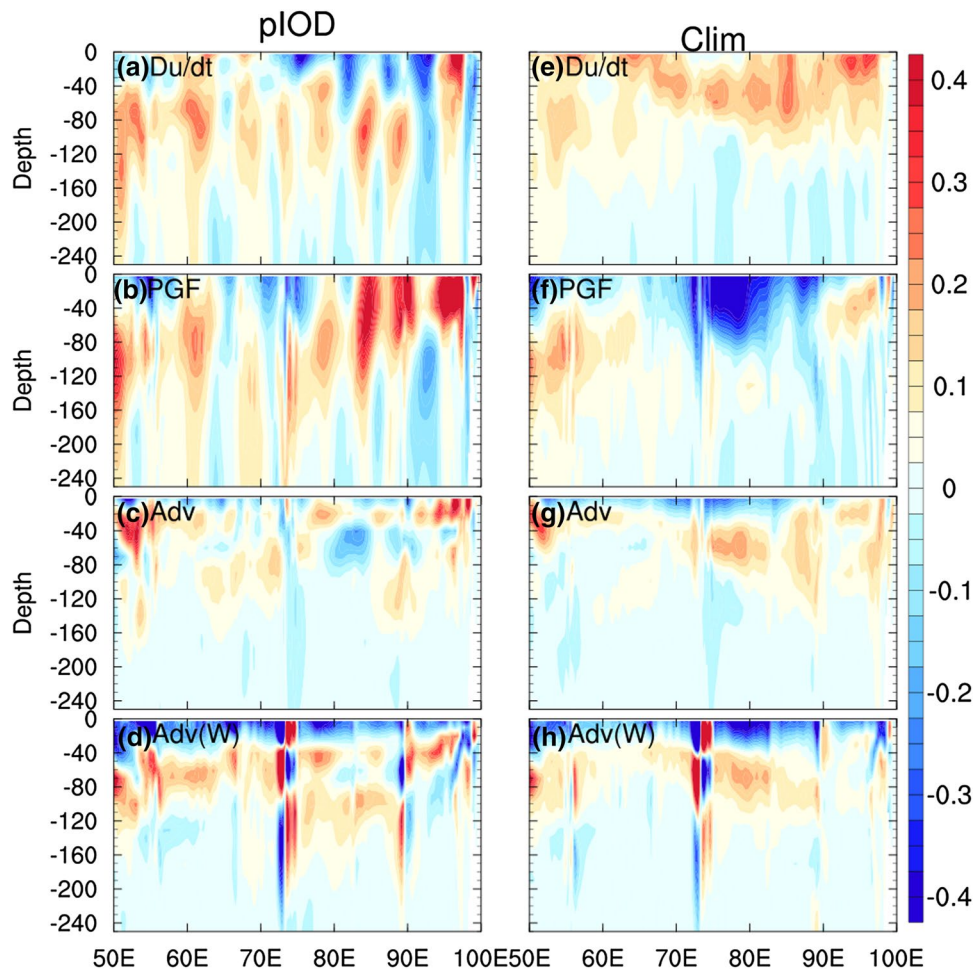
subsurface, and the vertical momentum advection also plays a secondary role.

5.2 Impacts of temperature and salinity anomalies

As discussed above, the variation of the zonal current is dominated by the zonal pressure gradient force that is mainly determined by the density gradient in the ocean. As the function factors of the density of sea water, both temperature and salinity play a leading role in the ocean dynamics process by modulating vertical stratification, controlling the mixed layer depth and barrier layer thickness. For example,

previous studies investigated the salinity contribution to the momentum advection of the zonal currents and the salinity impact on the Wyrtki Jets and EUC of the equatorial Indian Ocean (Masson et al. 2003, 2004). In this section, we will examine the impact of temperature and salinity anomalies on both pressure gradient force and momentum advection using two sensitivity experiments, and investigate their dynamical role in EUC. As described in Sect. 2.1, we restart the model with nudging climatological temperature or salinity, and meanwhile nudging the monthly temperature or salinity of the control run during the model forward integration of pIOD years.

Fig. 10 Composited August–September mean zonal momentum budget components averaged over 0.5°S – 0.5°N for five positive IOD events (1982, 1994, 1997, 2006 and 2012) (left) and climatology (right). **a–d** The tendency of zonal current, the pressure gradient force, total momentum advection and vertical momentum advection term for pIOD events, respectively. **e–h** Same as **a–d**, but for climatology. The colors represent the magnitude of zonal momentum budget components in 10^{-6} m/s^2



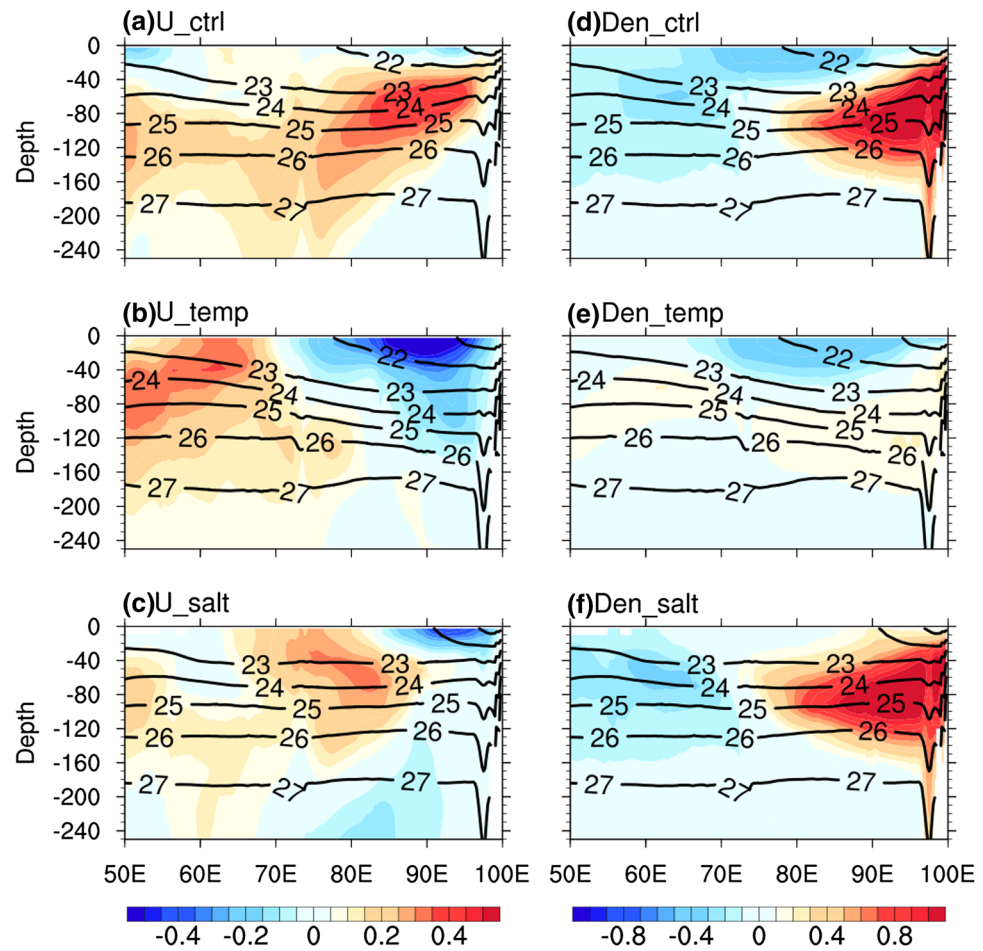
Shown in Fig. 11 are the composite of the zonal current and density anomalies along the equator, as a function of depth, in the two experiments for 5 positive IOD years used in above discussion. For comparison, the standard control run results analysed in preceding section are also presented here. As can be seen, the composite from the control run shows that EUC flows across the equatorial Indian Ocean under weak westward surface current, with its core encompassed by the isopycnal $\sigma_\theta = 23 \text{ kg/m}^3$ and $\sigma_\theta = 25.5 \text{ kg/m}^3$ (Fig. 11a). The positive density anomalies are strong in the east but weak in the west (Fig. 11d), which are mainly caused by the temperature anomalies as shown in Fig. 7a. Salinity anomalies in the central and eastern Indian Ocean may contribute to the negative density anomalies in the surface over that region (Figs. 7c, 11d).

In the temperature nudging experiment, as shown in U_temp in Fig. 11, the strong positive density anomalies in the subsurface vanish and only do the weak negative density anomalies induced by salinity exist in the surface (Fig. 11e). Under this situation, the eastward EUC disappears. The zonal currents are westward at the east of 75°E with the amplitude decreasing with depth, whereas the zonal

currents are eastward in the western equatorial Indian Ocean (Fig. 11b). In the salinity nudging experiment, although the weak negative density anomalies disappear in the surface over the central Indian Ocean, the strong positive density anomalies exist in the subsurface over the eastern equatorial Indian Ocean (Fig. 11f). Correspondingly, EUC still exists but is much weak (Fig. 11c). The above results suggest that subsurface temperature anomalies over the eastern Indian Ocean contribute most to the anomalous EUC. The salinity anomalies in the surface over the central Indian Ocean also play a secondary role in enhancing the EUC. As discussed in the previous studies (Thompson et al. 2006; Nyadjro and McPhaden 2014; Zhang et al. 2014; Chen et al. 2016), EUC can feed and intensify the upwelling off the Sumatra-Java coast and provide a positive feedback to the development of IOD events. The present study indicates that subsurface temperature anomalies over the eastern Indian Ocean and the surface salinity anomalies over the central Indian Ocean may favour the development of IOD by intensifying the EUC.

Similar to Fig. 10, we also conduct composite analysis of the budget components of August–September for the two nudging experiments, as shown in Fig. 12. In the temperature

Fig. 11 Composited SON mean zonal current and density anomalies averaged over 0.5°S – 0.5°N from the control run (upper: **a**, **d**), temperature nudging experiment (middle: **b**, **e**) and salinity nudging experiment (bottom: **c**, **f**). The colors represent zonal current (**a**–**c**) and density anomalies (**d**–**f**), respectively, and the contours represent the isopycnals. The temperature (salinity) nudging experiment mean the climatologically annual mean monthly temperature (salinity) is nudged during the entire integration of model



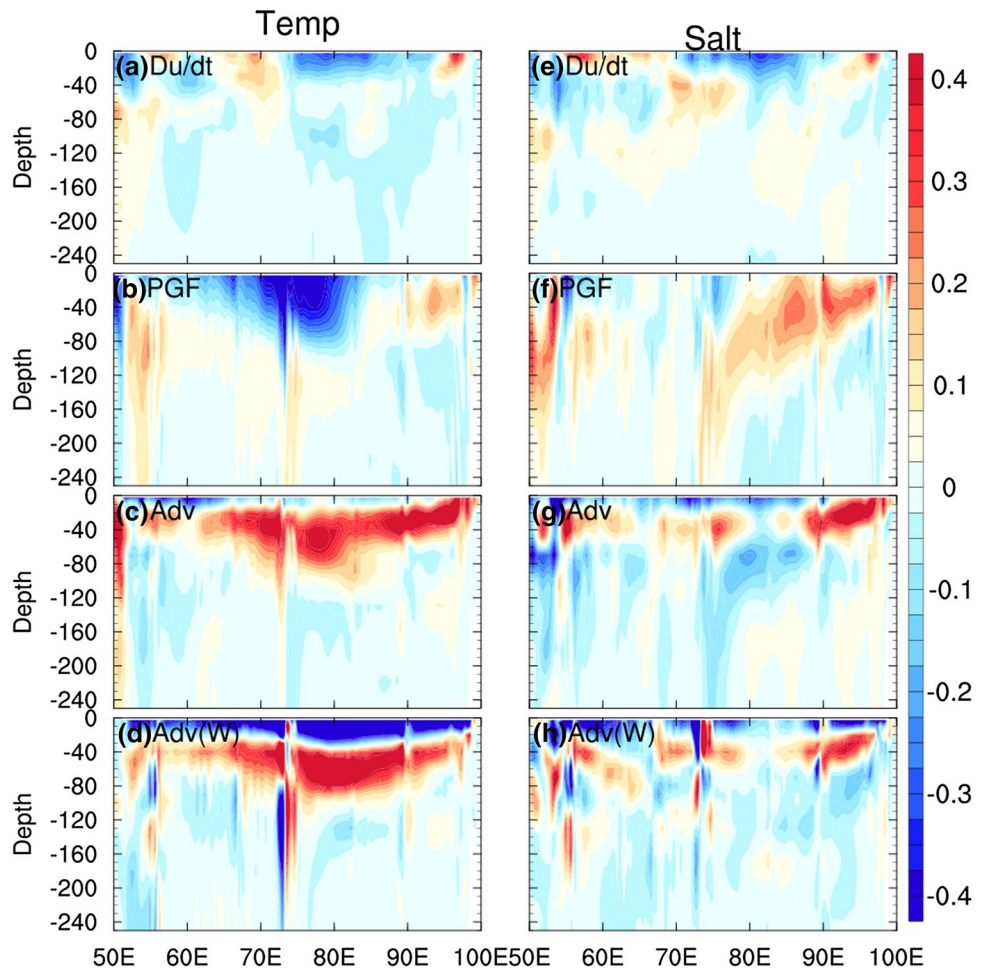
nudging experiment, the tendency of zonal current is negative in the upper 120 m east of 70°E , particularly in the subsurface layer where eastward acceleration disappears (Fig. 12a). The pressure gradient force has a pattern very similar to that of the climatology, where weak positive surface pressure gradient force only occurs east of 85°E and is negative in the central and western equatorial Indian Ocean, and its impact can be ignored below 80 m (Fig. 12b). This is completely different from that of control run (Fig. 10b), simply because there are no strong density anomalies exist along the equator after the temperature anomalies have been removed (Fig. 11d, e). In this temperature nudging experiment, the change of total momentum advection term is also apparent, with stronger eastward acceleration between 20 and 80 m due mainly to the contribution from the vertical momentum advection term (Fig. 12c, d). In the subsurface, however, the variation of total momentum advection term is relatively small. This suggests that the temperature anomalies in the eastern equatorial Indian Ocean significantly impact the pressure gradient force in the subsurface, playing an important role in driving the EUC.

The negative density anomalies in the control run have been disappeared in the salinity nudging experiment

(Fig. 11d, f), and the eastward acceleration of the zonal current also weakens in the subsurface that is contributed from both the pressure gradient force and total momentum advection term (Fig. 12e–g). Although the subsurface pressure gradient force in the eastern equatorial Indian Ocean is positive, it is much smaller than that in the control run (Fig. 12f). Compared with the control run, the positive total momentum advection becomes negative in the subsurface, and the contribution from the total momentum advection term, particularly the vertical momentum advection term, decelerates the eastward extension of EUC (Fig. 12g–h).

To examine the dynamical process of temperature and salinity anomalies in affecting the EUC in the eastern equatorial Indian Ocean through the changes in the pressure gradient force and total momentum advection term during the pIOD events, we conduct composite analysis of zonal current averaged over 75°E – 95°E , as shown in Fig. 13. During the pIOD events, strong EUC flows eastward in the subsurface under the weak westward surface currents between 2°S and 2°N (Fig. 13a). As discussed above, both the pressure gradient force and the total momentum advection accelerate the eastward zonal current in the subsurface (Fig. 13b). As shown in Fig. 13d, the

Fig. 12 Same as Fig. 10, but for the temperature (left) and salinity (right) nudging experiment

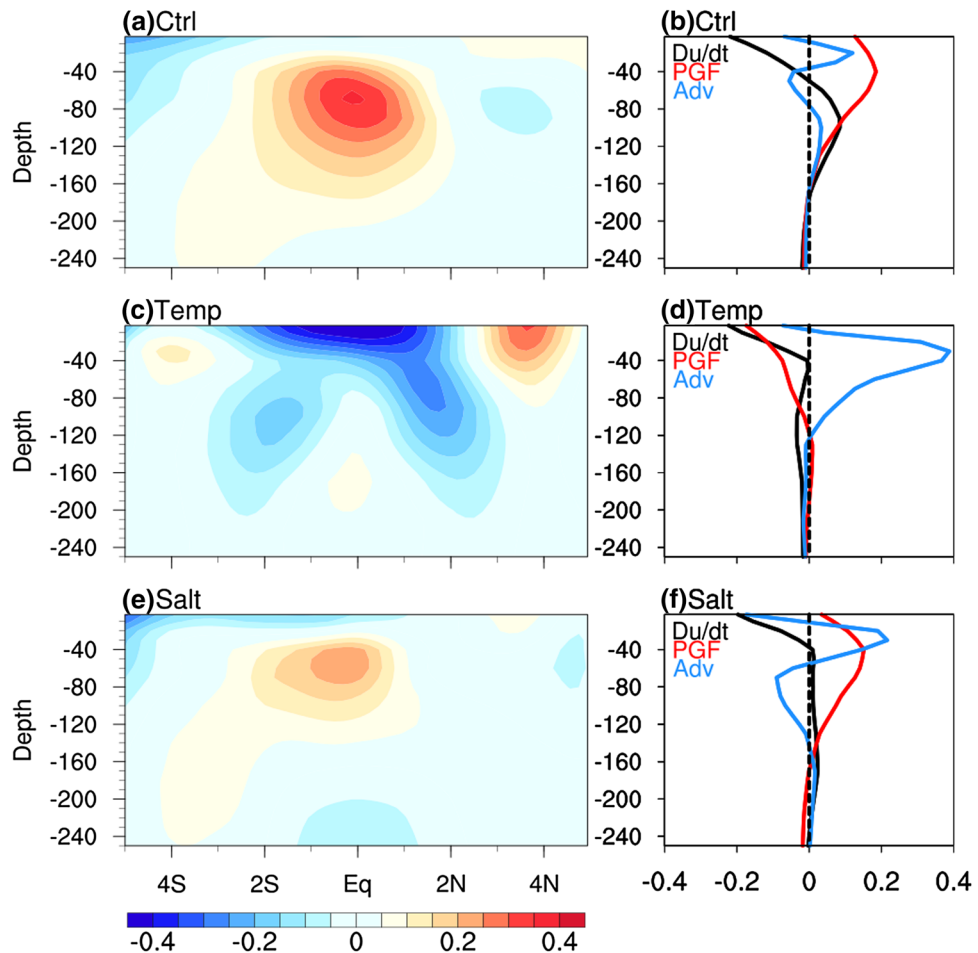


pressure gradient force changes to westward while the temperature is nudged to the climatology in the temperature nudging experiment, thereby the westward zonal current driven by the anomalous easterlies is enhanced in the surface (Fig. 13c, d). Also, the tendency of the zonal current impedes the generation of EUC due to the absence of eastward pressure gradient force in the subsurface. Compared with the control run, the eastward pressure gradient force slightly decreases and the EUC still exists but with a much weaker amplitude in the salinity nudging experiment, suggesting that the existence of eastward pressure gradient force is the main factor to drive the EUC (Fig. 13e, f). In addition, the total momentum advection decelerates the eastward EUC, indicating that the surface salinity anomalies in the central and eastern equatorial Indian Ocean not only increase the density gradient in the eastern Indian Ocean but also impact the momentum advection in the subsurface.

We further averaged the momentum advection components of August–September within the EUC core (80–160 m) along the central equatorial Indian Ocean (75°E–95°E, 0.5°S–0.5°N) in each nudging experiment, to investigate the

contribution of each term in the subsurface (Fig. 14). As shown in Fig. 14a, b, the averaged total momentum advection accelerates the zonal currents in the central equatorial Indian Ocean during the pIOD events and the acceleration is stronger in the temperature nudging experiment than in the control run, whereas the opposite variations are observed in the salinity nudging experiment. In the control run, the vertical momentum advection contributes most of total momentum advection to the acceleration of zonal current (Fig. 14c, d). The importance of vertical momentum advection can also be found in the temperature and salinity nudging experiment, where the vertical momentum advection dominates the variation of total momentum advection in the central equatorial Indian Ocean (Fig. 14e–h). It should be noted that the vertical momentum advection plays an important role in decelerating the zonal current in the salinity nudging experiment. In short, both temperature and salinity anomalies impact the total momentum advection in the subsurface in the central equatorial Indian Ocean, however, the salinity anomalies play an active role in enhancing the eastward acceleration through its impact on vertical momentum advection.

Fig. 13 Composited SON mean zonal current averaged over 75°E–95°E from the control run (a), temperature nudging experiment (c) and salinity nudging experiment (e). Vertical distribution of the mean zonal momentum budget components of August–September averaged over the central equatorial Indian Ocean (75°E–95°E, 0.5°S–0.5°N) from the control run (b), temperature nudging experiment (d) and salinity nudging experiment (f). The black, red and blue line indicate the tendency of zonal current, the pressure gradient force and total momentum advection, respectively. The magnitude of zonal momentum budget components is in 10^{-6} m/s^2



6 Summary and discussion

In this study, we focus on the transient variation of the EUC in the equatorial Indian Ocean. The emphasis is placed on the links of the EUC features to the IOD events and the possible physical process responsible for such links. This is conducted by a comprehensive analysis using observation, reanalysis and high-quality simulation. On the basis, the zonal momentum budget is dynamically diagnosed along the equatorial Indian Ocean. Further, two sensitivity experiments are conducted to investigate the role played by the temperature and salinity anomalies in driving and enhancing the eastward EUC, which intermittently appears in the subsurface during the pIOD events.

The results show that the core of EUC lies between 80 and 160 m. The EUC appears along the entire equatorial Indian Ocean during January–March in all years. However, during the summer–autumn, EUC can extend to the eastern Indian Ocean only during the pIOD events. It was found that the intensification and eastward extension of the transient EUC in the autumn during the pIOD events are always

accompanied by strong negative subsurface temperature anomalies in the eastern Indian Ocean and surface salinity anomalies in the central Indian Ocean.

The zonal momentum budget diagnosis shows that the pressure gradient force plays an important role in the variation of the tendency of zonal currents in the subsurface, and the vertical momentum advection term also plays a secondary role. During the pIOD events, the autumn subsurface EUC is mainly driven by the eastward pressure gradient force. The sensitivity experiments show that the positive subsurface density anomalies in the eastern Indian Ocean are mainly caused by the temperature anomalies, whereas the surface salinity anomalies in the central and eastern Indian Ocean contribute to the negative density anomalies over that region. In addition, our results also suggest that the temperature anomalies most significantly impact the pressure gradient force, and the surface salinity anomalies can also enhance the amplitude of EUC through increasing the density gradient in the eastern Indian Ocean and impacting the vertical momentum advection in the subsurface.

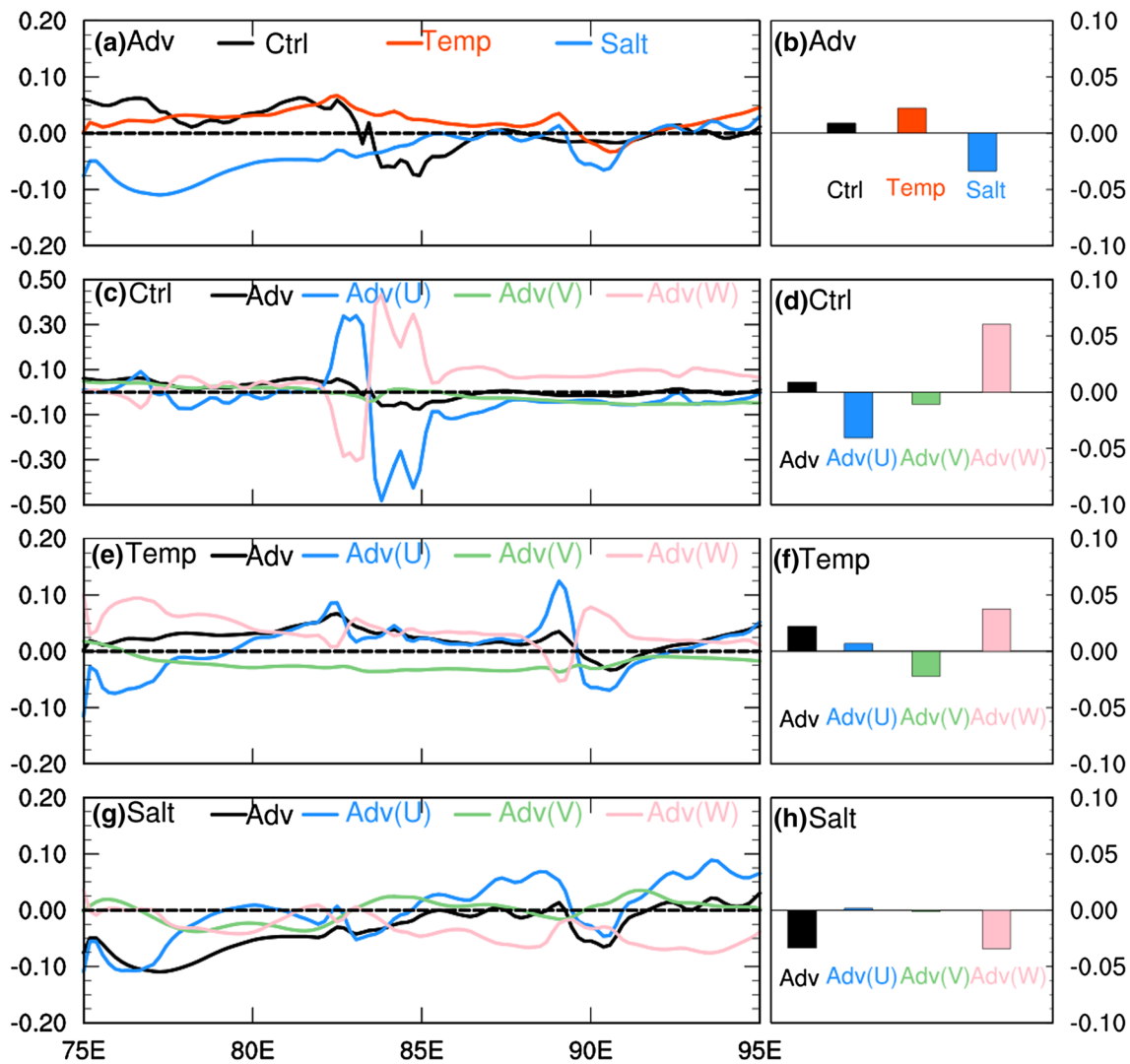


Fig. 14 **a** Distribution of the August–September mean momentum advection averaged between 80 m and 160 m, along the central equatorial Indian Ocean (75°E–95°E, 0.5°S–0.5°N) in the control run (black line), temperature nudging experiment (red line) and salinity nudging experiment (blue line). **b** Zonally averaged each item of **a**. **c**, **d** The distribution of the total momentum advection (black line and

bar), zonal momentum advection ($-\bar{u} \frac{\partial \bar{u}}{\partial x}$, blue line and bar), meridional momentum advection ($-\bar{v} \frac{\partial \bar{u}}{\partial y}$, green line and bar) and vertical momentum advection ($-\bar{w} \frac{\partial \bar{u}}{\partial z}$, pink line and bar) in the control run, respectively. **e–h** Same as **c, d**, but for the temperature nudging experiment and salinity nudging experiment, respectively. The magnitude of zonal momentum budget components is in 10^{-6} m/s^2

The mechanism and physical process responsible for the summer–autumn EUC anomalies during the pIOD events can be demonstrated by Fig. 15. During the pIOD events, the anomalous easterlies drive strong westward surface currents in the eastern Indian Ocean and push warm water westward. The equatorial upwelling Kelvin waves forced by the zonal winds propagate eastward, which tilts the thermocline zonally along the equator and drives the eastward pressure gradient. In the surface, the eastward pressure gradient is balanced by the zonal wind stress. The wind stress is small in the subsurface, and the pressure gradient is unbalanced, driving an eastward EUC. Meanwhile, the westward surface

currents advect fresh water from the Sumatra-Java coast and the Bay of Bengal into the central and eastern equatorial Indian Ocean, which results in negative surface salinity anomalies, and contributes to the reinforcement of the EUC.

The dynamical mechanisms of the EUC and the impact of IOD on it have drawn a broad attention in recent years. The role of Kelvin, Rossby waves and the summer monsoon in the formation and development of EUC has been well addressed in literatures. In this study, we analyze the EUC anomalies and explored the associated temperature and salinity anomalies, with an emphasis on these anomalies during the pIOD events. The results show that the subsurface

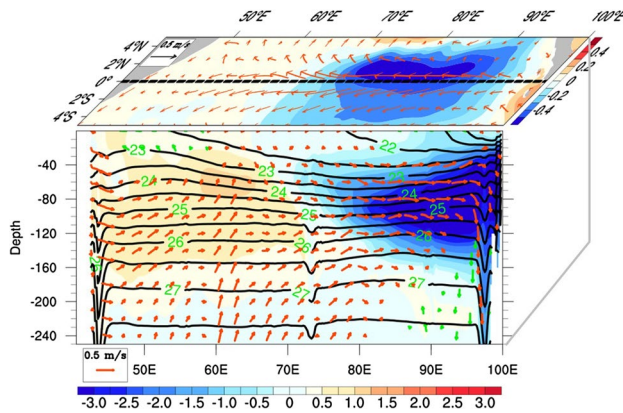


Fig. 15 3-dimenisoal diagrams of the dynamical process of the EUC averaged over September–November during positive IOD events (1982, 1994, 1997, 2006 and 2012). In the top surface (horizontal), the color represents the salinity anomalies averaged in the upper 80 m whereas the red vectors indicate the surface currents. In the front section (vertical), the color shows the temperature anomalies along the equator and the contour and vector represent the isopycnal and the zonal circulation, respectively. The scale for the current is 0.5 m/s

temperature anomalies over the eastern Indian Ocean play an important role in driving the EUC to extend eastward, and the salinity anomalies in the surface over the central Indian Ocean play a secondary role in enhancing the EUC. However, the dynamical mechanisms of the EUC are complicated and need to further study. In addition, it is also important to study the positive feedback process of EUC to IOD towards a fully understanding to the dynamics of IOD and the air–sea interaction, which is under our study.

Acknowledgements This study was supported by grants from the National Key R&D Program of China (2016YFC1401703), the Scientific Research Fund of the Second Institute of Oceanography, SOA (No. JG1707), the National Natural Science Foundation of China (Nos. 41706008, 41530961, 41690124, 41606012, 41690121, 41690120, 41621064, 41705049), the Project of State Key Laboratory of Satellite Ocean Environment Dynamics, Second Institute of Oceanography (No. SOEDZZ1516, SOEDZZ1701), the National Programme on Global Change and Air–Sea Interaction (GASI-IPOVAI-06). Y.T is also supported by the NSERC (Natural Sciences and Engineering Research Council of Canada) Discovery Grant. We thank two anonymous reviewers for their constructive comments that helped us to improve the manuscript.

Open Access This article is distributed under the terms of the Creative Commons Attribution 4.0 International License (<http://creativecommons.org/licenses/by/4.0/>), which permits unrestricted use, distribution, and reproduction in any medium, provided you give appropriate credit to the original author(s) and the source, provide a link to the Creative Commons license, and indicate if changes were made.

References

- Ashok K, Guan Z, Yamagata T (2001) Impact of the Indian Ocean dipole on the relationship between the Indian monsoon rainfall and ENSO. *Geophys Res Lett* 28:4499–4502. doi:[10.1029/2000GL013294](https://doi.org/10.1029/2000GL013294)
- Balmaseda MA, Mogensen K, Weaver AT (2013) Evaluation of the ECMWF ocean reanalysis system ORAS4. *Q J R Meteorol Soc* 139:1132–1161. doi:[10.1002/qj.2063](https://doi.org/10.1002/qj.2063)
- Behera SK, Luo J-J, Masson S, Delecluse P, Gualdi S, Navarra A, Yamagata T (2005) Paramount impact of the Indian ocean dipole on the East African short rains: a CGCM study. *J Clim* 18:4514–4530. doi:[10.1175/JCLI3541.1](https://doi.org/10.1175/JCLI3541.1)
- Cai W, Cowan T, Raupach M (2009) Positive Indian Ocean Dipole events precondition southeast Australia bushfires. *Geophys Res Lett* 36:L19710. doi:[10.1029/2009GL039902](https://doi.org/10.1029/2009GL039902)
- Cai W, Van Rensch P, Cowan T, Hendon HH (2011) Teleconnection pathways of ENSO and the IOD and the mechanisms for impacts on Australian rainfall. *J Clim* 24:3910–3923. doi:[10.1175/2011JCLI4129.1](https://doi.org/10.1175/2011JCLI4129.1)
- Carton JA, Giese BS (2008) A reanalysis of ocean climate using simple ocean data assimilation (SODA). *Mon Weather Rev* 136:2999–3017. doi:[10.1175/2007MWR1978.1](https://doi.org/10.1175/2007MWR1978.1)
- Chen G, Han W, Li Y, Wang D, McPhaden MJ (2015) Seasonal-to-interannual time-scale dynamics of the equatorial undercurrent in the Indian ocean. *J Phys Oceanogr* 45:1532–1553. doi:[10.1175/IPO-D-14-0225.1](https://doi.org/10.1175/IPO-D-14-0225.1)
- Chen G, Han W, Shu Y, Li Y, Wang D, Xie Q (2016) The role of equatorial undercurrent in sustaining the Eastern Indian Ocean upwelling. *Geophys Res Lett* 43:6444–6451. doi:[10.1002/2016GL069433](https://doi.org/10.1002/2016GL069433)
- Dai A, Trenberth KE (2002) Estimates of freshwater discharge from continents: latitudinal and seasonal variations. *J Hydrometeorol* 3:660–687
- Feng R, Duan W, Mu M (2014) The “winter predictability barrier” for IOD events and its error growth dynamics: results from a fully coupled GCM. *J Geophys Res* 119:8688–8708. doi:[10.1002/2014JC010473](https://doi.org/10.1002/2014JC010473)
- Grodsky SA, Carton JA, Murtugudde R (2001) Anomalous surface currents in the tropical Indian Ocean. *Geophys Res Lett* 28:4207–4210. doi:[10.1029/2001GL013592](https://doi.org/10.1029/2001GL013592)
- Grunseich G, Subrahmanyam B, Murty VSN, Giese BS (2011) Sea surface salinity variability during the Indian Ocean Dipole and ENSO events in the tropical Indian Ocean. *J Geophys Res* 116:C11013. doi:[10.1029/2011JC007456](https://doi.org/10.1029/2011JC007456)
- Guo F, Liu Q, Sun S, Yang J (2015) Three types of Indian Ocean dipoles. *J Clim* 28:3073–3092. doi:[10.1175/JCLI-D-14-00507.1](https://doi.org/10.1175/JCLI-D-14-00507.1)
- Han W, Webster P, Lukas R, Hacker P, Hu A (2004) Impact of atmospheric intraseasonal variability in the Indian Ocean: low-frequency rectification in equatorial surface current and transport. *J Phys Oceanogr* 34:1350–1372. doi:[10.1175/1520-0485\(2004\)034<1350:IOAIVI>2.0.CO;2](https://doi.org/10.1175/1520-0485(2004)034<1350:IOAIVI>2.0.CO;2)
- Hashizume M, Chaves LF, Minakawa N (2012) Indian Ocean dipole drives malaria resurgence in East African highlands. *Sci Rep* 2:269. doi:[10.1038/srep00269](https://doi.org/10.1038/srep00269)
- Iskandar I, Masumoto Y, Mizuno K (2009) Subsurface equatorial zonal current in the eastern Indian Ocean. *J Geophys Res* 114:C06005. doi:[10.1029/2008JC005188](https://doi.org/10.1029/2008JC005188)
- Itzumo T (2005) The equatorial undercurrent, meridional overturning circulation, and their roles in mass and heat exchanges during El Niño events in the tropical Pacific ocean. *Ocean Dyn* 55:110–123. doi:[10.1007/s10236-005-0115-1](https://doi.org/10.1007/s10236-005-0115-1)
- Knox RA (1976) On a long series of measurements of Indian Ocean equatorial currents near Addu Atoll. *Deep Sea Res* 23:211–221. doi:[10.1016/0011-7471\(76\)91325-5](https://doi.org/10.1016/0011-7471(76)91325-5)

- Krishnan R, Swapna P (2009) Significant influence of the boreal summer monsoon flow on the Indian Ocean response during dipole events. *J Clim* 22:5611–5634. doi:[10.1175/2009JCLI2176.1](https://doi.org/10.1175/2009JCLI2176.1)
- Li J, Liang C, Tang Y, Dong C, Chen D, Liu X, Jin W (2016) A new dipole index of the salinity anomalies of the tropical Indian Ocean. *Sci Rep* 6:24260. doi:[10.1038/srep24260](https://doi.org/10.1038/srep24260)
- Liu X, Dong C, Chen D, Su J (2014) The pattern and variability of winter Kuroshio intrusion northeast of Taiwan. *J Geophys Res Oceans* 119:5380–5394. doi:[10.1002/2014JC009879](https://doi.org/10.1002/2014JC009879)
- Masson S, Menkes C, Delecluse P, Boulanger J-P (2003) Impacts of salinity on the eastern Indian Ocean during the termination of the fall Wyrtki Jet. *J Geophys Res* 108:3067. doi:[10.1029/2001JC000833](https://doi.org/10.1029/2001JC000833)
- Masson S, Boulanger JP, Menkes C, Delecluse P, Yamagata T (2004) Impact of salinity on the 1997 Indian Ocean dipole event in a numerical experiment. *J Geophys Res* 109:C02002. doi:[10.1029/2003JC001807](https://doi.org/10.1029/2003JC001807)
- McPhaden M (1982) Variability in the central equatorial Indian Ocean. I. Ocean dynamics. *J Mar Res* 40:157–176
- McPhaden MJ (1986) Equatorial undercurrent: 100 years of discovery. *Eos. Trans Am Geophys Union* 67:762–765. doi:[10.1029/EO067i040p00762](https://doi.org/10.1029/EO067i040p00762)
- McPhaden MJ, Meyers G, Ando K, Masumoto Y, Murty VSN, Ravichandran M, Syamsudin F, Vialard J, Yu L, Yu W (2009) RAMA: the research moored array for African–Asian–Australian monsoon analysis and prediction. *Bull Am Meteor Soc* 90:459–480. doi:[10.1175/2008BAMS2608.1](https://doi.org/10.1175/2008BAMS2608.1)
- McPhaden MJ, Wang Y, Ravichandran M (2015) Volume transports of the Wyrtki jets and their relationship to the Indian Ocean Dipole. *J Geophys Res* 120:5302–5317. doi:[10.1002/2015JC010901](https://doi.org/10.1002/2015JC010901)
- Murtugudde R, McCreary JP, Busalacchi AJ (2000) Oceanic processes associated with anomalous events in the Indian Ocean with relevance to 1997–1998. *J Geophys Res Ocean* 105:3295–3306. doi:[10.1029/1999JC900294](https://doi.org/10.1029/1999JC900294)
- Nagura M, McPhaden MJ (2014) Zonal momentum budget along the equator in the Indian Ocean from a high-resolution ocean general circulation model. *J Geophys Res* 119:4444–4461. doi:[10.1002/2014JC009895](https://doi.org/10.1002/2014JC009895)
- Nyadjro ES, McPhaden MJ (2014) Variability of zonal currents in the eastern equatorial Indian Ocean on seasonal to interannual time scales. *J Geophys Res Oceans* 119:7969–7986. doi:[10.1002/2014JC010380](https://doi.org/10.1002/2014JC010380)
- Reppin J, Schott FA, Fischer J, Quadfasel D (1999) Equatorial currents and transports in the upper central Indian Ocean: Annual cycle and interannual variability. *J Geophys Res Oceans* 104:15495–15514. doi:[10.1029/1999JC900093](https://doi.org/10.1029/1999JC900093)
- Roemmich D, Gilson J (2009) The 2004–2008 mean and annual cycle of temperature, salinity, and steric height in the global ocean from the Argo program. *Prog Oceanogr* 82:81–100. doi:[10.1016/j.pocean.2009.03.004](https://doi.org/10.1016/j.pocean.2009.03.004)
- Saha S et al (2010) The NCEP Climate Forecast System Reanalysis. *Bull Am Meteor Soc* 91:1015–1057. doi:[10.1175/2010BAMS3001.1](https://doi.org/10.1175/2010BAMS3001.1)
- Saha S et al (2014) The NCEP climate forecast system version 2. *J Clim* 27:2185–2208. doi:[10.1175/JCLI-D-12-00823.1](https://doi.org/10.1175/JCLI-D-12-00823.1)
- Saji N, Yamagata T (2003a) Structure of SST and surface wind variability during Indian Ocean dipole mode events: COADS observations. *J Clim* 16:2735–2751. doi:[10.1175/1520-0442\(2003\)016<2735:SOSASW>2.0.CO;2](https://doi.org/10.1175/1520-0442(2003)016<2735:SOSASW>2.0.CO;2)
- Saji N, Yamagata T (2003b) Possible impacts of Indian Ocean Dipole mode events on global climate. *Clim Res* 25:151–169. doi:[10.3354/cr025151](https://doi.org/10.3354/cr025151)
- Saji N, Goswami B, Vinayachandran P, Yamagata T (1999) A dipole mode in the tropical Indian Ocean. *Nature* 401:360–363
- Schott FA, McCreary JP Jr (2001) The monsoon circulation of the Indian Ocean. *Prog Oceanogr* 51:1–123. doi:[10.1016/S0079-6611\(01\)00083-0](https://doi.org/10.1016/S0079-6611(01)00083-0)
- Shchepetkin AF, McWilliams JC (2005) The regional oceanic modeling system (ROMS): a split-explicit, free-surface, topography-following-coordinate oceanic model. *Ocean Model* 9:347–404
- Smith WHF, Sandwell DT (1997) Global sea floor topography from satellite altimetry and ship depth soundings. *Science* 277:1956–1962
- Swapna P, Krishnan R (2008) Equatorial undercurrents associated with Indian Ocean Dipole events during contrasting summer monsoons. *Geophys Res Lett* 35:L14S04. doi:[10.1029/2008GL033430](https://doi.org/10.1029/2008GL033430)
- Thompson B, Gnanaseelan C, Salvekar P (2006) Variability in the Indian Ocean circulation and salinity and its impact on SST anomalies during dipole events. *J Mar Res* 64:853–880
- Ummenhofer CC, England MH, McIntosh PC, Meyers GA, Pook MJ, Risbey JS, Gupta AS, Taschetto AS (2009) What causes southeast Australia's worst droughts? *Geophys Res Lett* 36:L04706. doi:[10.1029/2008GL036801](https://doi.org/10.1029/2008GL036801)
- Webster PJ, Moore AM, Loschnigg JP, Leben RR (1999) Coupled ocean–atmosphere dynamics in the Indian Ocean during 1997–98. *Nature* 401:356–360
- Wyrtki K (1973) An equatorial jet in the Indian Ocean. *Science* 181:262–264. doi:[10.1126/science.181.4096.262](https://doi.org/10.1126/science.181.4096.262)
- Yao Z, Tang Y, Chen D, Zhou L, Li X, Lian T, Ul Islam S (2016) Assessment of the simulation of Indian Ocean Dipole in the CESM-Impacts of atmospheric physics and model resolution. *J Adv Model Earth Syst* 8:1932–1952. doi:[10.1002/2016MS000700](https://doi.org/10.1002/2016MS000700)
- Zhang Y, Du Y, Zheng S, Yang Y, Cheng X (2013) Impact of Indian Ocean dipole on the salinity budget in the equatorial Indian Ocean. *J Geophys Res* 118:4911–4923. doi:[10.1002/jgrc.20392](https://doi.org/10.1002/jgrc.20392)
- Zhang D, McPhaden MJ, Lee T (2014) Observed interannual variability of zonal currents in the equatorial Indian Ocean thermocline and their relation to Indian Ocean Dipole. *Geophys Res Lett* 41:7933–7941. doi:[10.1002/2014GL061449](https://doi.org/10.1002/2014GL061449)